applied system innovation

MDPI

Review

A Brief Description of Cyclic Voltammetry Transducer-Based Non-Enzymatic Glucose Biosensor Using Synthesized Graphene Electrodes

Mohamed Husien Fahmy Taha [1], Hager Ashraf [2] and Wahyu Caesarendra [3,*]

[1] Department of Continuing Education, University of Oxford, Oxford OX1 4BH, UK; mohamed.husienfahmytahaabdelrahman@conted.ox.ac.uk
[2] Department of Biochemistry, Alexandria University, Alexandria 21644, Egypt; hagerashraf2030@gmail.com
[3] Faculty of Integrated Technologies, Universiti Brunei Darussalam, Jalan Tungku Link, Gadong BE1410, Brunei Darussalam
* Correspondence: wahyu.caesarendra@ubd.edu.bn; Tel.: +673-7345-623

Received: 19 June 2020; Accepted: 27 July 2020; Published: 2 August 2020

Abstract: The essential disadvantages of conventional glucose enzymatic biosensors such as high fabrication cost, poor stability of enzymes, pH value-dependent, and dedicated limitations, have been increasing the attraction of non-enzymatic glucose sensors research. Beneficially, patients with diabetes could use this type of sensor as a fourth-generation of glucose sensors with a very low cost and high performance. We demonstrate the most common acceptable transducer for a non-enzymatic glucose biosensor with a brief description of how it works. The review describes the utilization of graphene and its composites as new materials for high-performance non-enzymatic glucose biosensors. The electrochemical properties of graphene and the electrochemical characterization using the cyclic voltammetry (CV) technique of electrocatalysis electrodes towards glucose oxidation have been summarized. A recent synthesis method of the graphene-based electrodes for non-enzymatic glucose sensors have been introduced along with this study. Finally, the electrochemical properties such as linearity, sensitivity, and the limit of detection (LOD) for each sensor are introduced with a comparison with each other to figure out their strengths and weaknesses.

Keywords: glucose detection; non-enzymatic sensor; cyclic voltammetry; graphene electrodes

1. Introduction

The conventional sensing methods in medicine and life sciences require expensive reagents, high-precision instruments, and quantitative methods to achieve highly sensitive detection. Thus, many novel nano-biosensors have been developed due to the need for early detection and diagnosis of the disease, as well as minimally invasive detection approaches [1–5]. The integration of biosensors with nanotechnology has facilitated the considerable progress of biosensor development. The nano-sized nature of nanomaterials and their unique chemical and electrical properties have promoted the enhancement of both selectivity and sensitivity at a very low concentration on the biosensors [1–3,6]. Generally, biosensors consist of three basic elements: Bioreactor, transducer, and detector. A bioreactor is an element that reacts with the analyte (bacteria, complementary DNA, antigen, etc.) in the form of (enzyme, DNA probe, antibacterial, etc.). The employment of enzymes is widely used in biosensors. It is also responsible for binding the dedicated form to the object (sample). With respect to the bioreactor elements and their interaction types, there are two types of sensors. Catalytic sensor—a signal that converts the substrate to a product after binding the analyte with biological elements without any chemical change A↔B where the transducer receives A or B input. Affinity sensor-biological elements and the analyte interact with each other and their output is the detected complex event A*B→AB where

the transducer reveals the complex interaction [7–9]. The transducer is an element which converts the (bio) chemical signal to an electrical signal to be measured. The principle of detection depends on the type of used transducer signal and biorecognition elements which lead directly to correlate with the analyte concentration inversely or proportionally [10]. The electronic system (detector) is responsible for receiving the transducer signal and amplifying it using a signal amplifier, and then sending it to be processed by the computer. The computer could read the amplified signal and convert it to readable data that have magnificent physical investigated parameters [7], as presented in Figure 1.

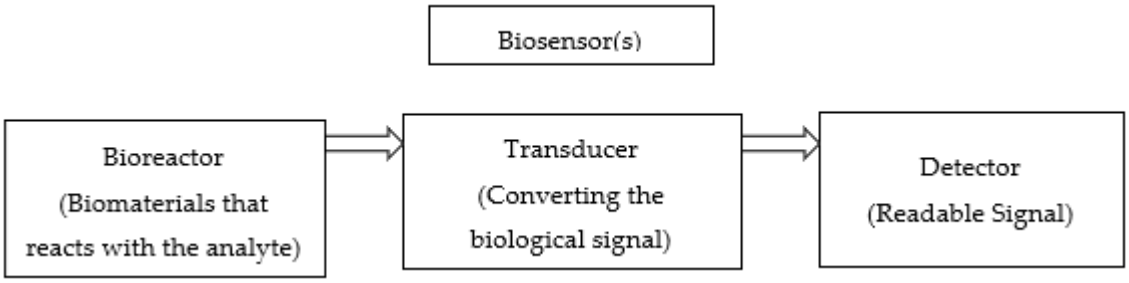

Figure 1. Block diagram of biosensors in order.

Nano-biosensors can be categorized according to the basic detection principles of signal transduction and biorecognition elements into three main types: (1) Electrochemical detection principles, (2) optical detection principles, and (3) mass detection principles [6]. In comparison with other detection approaches, electrochemical sensors for multiple analytes were the first scientifically proposed as well as successfully commercialized biosensors. This stems from several remarkable electrochemical abilities including the high sensitivity of electrochemical transducers (such as the cyclic voltammeter transducer), their compatibility with modern technologies, simplicity, and low detection limit [6,11]. The fundamental principle of electrochemical biosensors is that the chemical reaction between the immobilized biomolecule and target analyte produces or consume ions or electrons, which affects readable electrical properties of the solution such as electric current, voltage, and resistance. Each reaction can be represented by a simple electric circuit model and the electrochemical signal produced is then used to relate quantitatively to the amount of analyte [11,12].

The biosensors benchmarks depend on its linearity (maximum linear value of the sensor calibration curve responding to the glucose. Good linear sensors would detect high substrate concentrations), sensitivity (the value of the electrode response per substrate concentration. Highly sensitive sensors could be detected at low concentrations), selectivity (interference of chemicals must be minimized for obtaining the correct result), and response time (the necessary time for having 95% of the response).

The construction of electrochemical biosensors has been improved with the incorporation of carbon nanomaterial due to their feature size (1–100 nm), large surface-to-volume ratio, and high biocompatibility, thus contributing to the improvement of the analytical performance of such biosensors. In addition, carbon nanomaterials are advantageous because they enhance interfacial adsorption properties, increase electrocatalytic activity, and promote electron transfer kinetics compared to many conventional electrochemical biosensor materials [13,14].

Graphene is a planar sheet with a two-dimensional (2D) carbon nanomaterial hexagonal pattern [13,15]. The atomic thickness of the graphene sheet and its high surface-to-volume ration allow all carbon atoms to interact directly with the analytes, consequently making such material high sensitive towards the change of local environment conditions, thus promoting higher sensitivity than carbon nanotubes (CNTs) [5,14]. In opposition to CNTs, graphene has two main advantages regarding its application in electrochemical biosensors. Firstly, graphene does not contain metallic impurities, which interfere with the material electrochemistry and is considered the main drawback of CNTs. Further comprising, graphene compounds can be easily incorporated in biosensor fabrication while it is difficult in the case of CNTs due to its one-dimensional nature [5,14–16]. Moreover, graphene-derivatives nanocomposites

have the advantages of good stability, wide potential window, low reaction over potential, negligible residual current, and excellent electro-catalytic activity which are beneficial for the construction of high-performance electrochemical biosensors. Since the discovery of graphene was placed as a champion for biosensors electrode development thanks to its superior performance enhancement of the materials such as metals, metal oxides, etc. [5,13,17,18]. Carbonic nanostructures that include various low-dimensional allotropes of carbon including fullerene (0D), carbon nanotube (1D), carbon nano-onion, carbon nanohorn, nanodiamond, and graphene (2D) have unique electrochemical properties. In comparison to other carbon nanostructures graphene has recently been used in the construction of electrochemical biosensors due to its extraordinary characteristics including electrochemical reactivity, conductivity, mechanical strength, and low toxicity [5,11,13,14]. Different types of carbon allotropes crystalline have been presented in Figure 2.

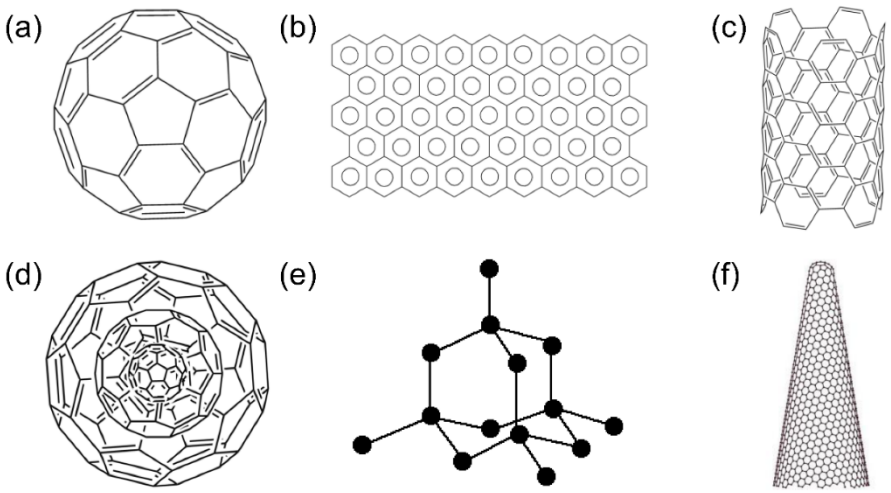

Figure 2. Different types of carbon allotropes crystalline. (**a**) Fullerene—C60, (**b**) graphene monolayer, (**c**) carbon nanotube (CNT), (**d**) carbon nano-onion, (**e**) nanodiamond, (**f**) carbon nanohorn.

1.1. History of Glucose Sensors

Clark and Lyons developed the first-generation of glucose sensors using an electrochemical method to monitor the oxygen consumed by the catalyzed enzyme. A thin layer of GOx enzyme, immobilized over the oxygen electrode, had been developed for that purpose [19]. The reaction could be described by the following equations:

$$Glucose + O_2 \rightarrow glucose\ acid + H_2O_2 \quad (1)$$

Reductive detection of oxygen consumption could be calculated by applying a negative potential to the cathode electrode:

$$O_2 + 4H + +4e- \rightarrow 2H_2O \quad (2)$$

In second-generation glucose sensors, mediators (soluble redox-active molecules have abilities of rapid and reversible redox reactions in which closure of the electrons between the redox center at the enzymatic active site and electrode surface) are developed to be used [20,21]. The following equations describe the second-generation glucose biosensors:

$$glucose + GOx(FAD) \rightarrow gluconic\ acid + GOx(FADH_2) \quad (3)$$

$$GOx(FADH_2) + 2\mathrm{M(ox)} + 2e^- \rightarrow GOx(FAD) + 2\mathrm{M(red)} + 2H^+ \quad (4)$$

$$2\mathrm{M(red)} \rightarrow\ 2\mathrm{M(ox)} + 2e^- \quad (5)$$

where M(ox) and M(red) are the oxidized and reduced forms of the mediator. The third-generation glucose biosensors operated with a direct electron transfer between the enzymatic redox center and electrode, which create high sensitivity and reproducibility without any mediators and at low potential [22–24]. The mechanism of this biosensor can be understood by the following reactions:

$$glucose + GOx(FAD) \rightarrow gluconic\ acid + GOx(FADH_2) \quad (6)$$

$$GOx(FADH_2) + 2e^- \rightarrow GOx(FAD) + 2H^+ \quad (7)$$

Figure 3 shows a schematic of the three generations of glucose sensors.

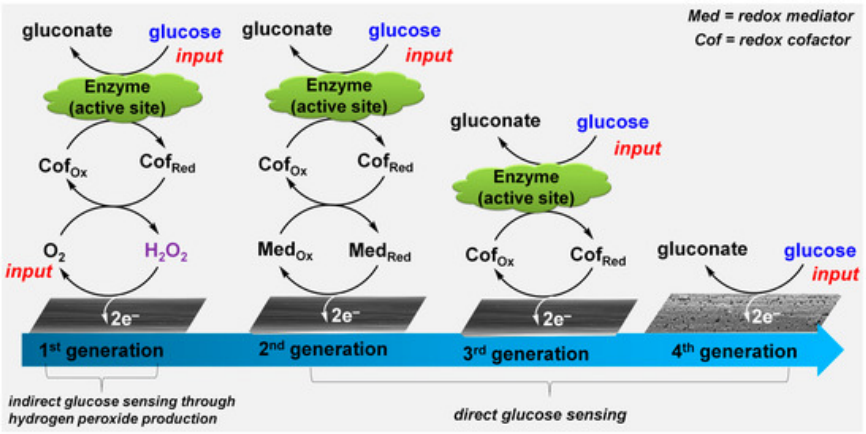

Figure 3. Summary of glucose electrooxidation mechanisms: Presented as enzymatic (first-, second-, and third-generation sensors) and non-enzymatic (so-called herein "fourth-generation" sensors).

1.2. Advantages of Glucose Sensing without the Enzyme

Enzymatic and non-enzymatic electrochemical glucometers are the two mainly glucose-sensing approaches. Enzymatic approaches, in principle, depend on the oxidation of glucose molecules by the utilization of recognition enzymes such as GO*x* or glucose dehydrogenase (GDH), which results in the generation of detectable compounds such as O_2, CO_2, or H_2O_2. The detection mechanism relies on typical current values relative to the concentration of the original glucose when interacting with the surface of the sensor. Although enzyme-based glucometers have dominated the industry of glucose biosensors for decades, there are several critical challenges that prohibit their further advancement. Particularly, they suffer from low thermal and chemical stability issues because of the enzymatic protein nature. Even if GO*x* is more stable than other enzymes, it is highly vulnerable to environmental factors such as pH (constrained to the pH range from 2 to 8), temperature (below 44 °C), and humidity levels. Moreover, the easy deactivation of GO*x* in the presence of some detergents such as sodium n-dodecyl sulfate at low pH and hexadecyltrimethylammonium bromide at high pH, leads to a quick deactivated GO*x* [25,26]. The instabilities of GO*x* chemically and thermally stand as a barrier for continuous monitoring during the fermentation process in the enzymatic biosensor. The stability of the enzymatic biosensor is required, which means complex fabrication strategies of the enzyme within the polymers, covalent cross-linking of the enzyme, sol-gel entrapment of enzyme, etc. [26–29].

Three generations of glucose biosensors suffered from the arising limitation of the performance where the sensors depend on pH value, enzyme activity and interference, electrode surrounding, (temperature and humidity), etc. The short-term stability of enzymatic glucose sensors creates a problem for the users (single-time disposable usage), in addition, it is not possible to avoid the harsh thermal and chemical conditions during the fabrication, storage, and usage of enzymatic glucose sensors. The high-cost fabrication and short lifetime of enzymatic glucose biosensors are problems for most diabetes patients, and this explains why non-enzymatic glucose biosensors attract extraordinary research interest.

The non-enzymatic glucose biosensors are promising for the fourth-generation of analytical GOx, in which the electrodes can oxidize the glucose in the sample without enzymatic needs [30,31]. However, the non-enzymatic glucose biosensor is based on the electrocatalysts activity to oxide the glucose without enzymes, such as metals (Au, Ni, Cu, Pd, etc.), metal oxides (CuO, RuO2, etc.), alloys (PtPb, PtRu, etc.), complex (nickel hexacyanoferrate, etc.), and carbon (graphene, diamond, nanotubes, etc.).

Investigating the right material composition of the electrodes are the keywords to get a good output of these types of biosensors such as high sensitivity, low cost, and stability. Recently emerging, a class of graphene-based non-enzymatic glucose sensor electrodes with nanoparticles, metals, metal oxides, alloys, and polymers would meet these scientific demands such as cost-effectiveness, synthesis approach, biocompatibility, stability, electron-transfer kinetics, and sensitivity [32–37].

2. Electrochemical Properties of Graphene, Graphene Oxide (GO), and Reduced Graphene Oxide (rGO)

Materials with extraordinary electrochemical properties of graphene have appeared because of its bond structure (sp2 bonds) and the configuration (a hexagon configuration) such as a large surface area of about 2630 m^2g^{-1}, a controlled bandgap, and high conductivity theoretically about 0.96×10^6 $ohm\,cm^{-1}$ ($200,000\,cm^2v^{-1}\,s^{-1}$ $electron\ mobility$) [38,39]. While the graphene is a semiconductor with zero bandgap, graphene oxide (GO) and reduced graphene oxide (rGO) have band gaps of about 2.2 and 1.00–1.69 eV, consequently [40]. The highly oriented pyrolytic graphene (HOPG) has an electron transfer rate of the edged plane of graphene that is about 0.01 cm/s, while the basal plane is about below 10^{-9} cm/s. Since the graphene electrochemical properties could be controlled by its edge where the heterogeneous electron transfer (HET) is fast, the graphene nanocomposites are good electrodes for non-enzymatic glucose sensors [41].

A large π bond of poly atoms throughout the entire layer is due to the electrons in the ps2 orbitals that are perpendicular to the plane of the layer of each carbon, which makes graphene possess excellent electrochemical properties such as high conductivity at room temperature and current-voltage characteristics. Moreover, the π-π stacking and hydrophobic interactions enhance the connection of graphene to biomolecules [8,10,42].

Solution-processability of graphene is more suitable for biosensing applications, due to its compatibility with biochemical systems and inexpensive cost [7,8,10,43]. In addition to the electronic properties such as semi-metallic properties, a strong bipolar electric field effect with a high concentration of charge carriers, a small overlap of band gaps, and a quantum hall effect, graphene also has unique mechanical properties such as bandgap tenability, high elasticity, and excellent heat transfer [10]. Hence, a variety of graphene-based materials were prepared and successfully used in designing electrochemical biosensors such as graphene oxide (GO) and reduced graphene oxide (rGO) (see Section 5).

GO and rGO are widely used in non-enzymatic glucose sensors because of their electrochemical properties. The basal plate of GO including the oxygenated groups (epoxy, hydroxyl) have an electrochemical advantage that increase surface functionalization to attract the target, while the decrease of electrical conductivity is due to insulation from oxygenated groups standing as a barrier. The limit of the insulation directly depends on the oxidation level [44–47]. In fact, due to the decrease in electrical conductivity, rGO replaced GO in many electrochemical sensors especially non-enzymatic glucose sensors. By reducing the oxygen-containing groups using many approaches such as electrochemically and hydrothermally, that makes the electrochemical properties much better. Furthermore, the electrical properties of rGO are highly dependent on the reduction methods [48–51]. Table 1 introduces a general idea of the graphene, GO, and rGO properties.

Table 1. Graphene, graphene oxide (GO), and reduced graphene oxide (rGO) properties in general.

Properties	Graphene	GO	rGO
Electron mobility @ room temperature	~200,000–250,000 cm^2 V^{-1} s^{-1}	0.1–10 cm^2 V^{-1} s^{-1}	2–200 cm^2 V^{-1} s^{-1}
Surface area	2630 m^2 g^{-1} [38]	736.6 m^2 g^{-1} [52]	466–758 m^2 g^{-1} [53,54]
Thermal conductivity	~5000 W m^{-1} K^{-1} [38,54]	0.5–18 W m^{-1} K^{-1} [55,56]	1390–2275 W m^{-1} K^{-1} [56–58]
Carbon-carbon bond length	0.142 nm [54–59]	N/A	N/A
Specific capacitance (depends on cyclic voltammetry)	550 F g^{-1} [60]	215–255 F g^{-1} [61]	210–425 F g^{-1} [60,62,63]
Electrical conductivity (depends on reduction technique)	~6×10^8 S m^{-1} [53,64]	5.7×10^{-6} S m^{-1} [62]	10^2–10^5 S m^{-1} [65–67]
Sheet resistance	200 Ω sq^{-1} [68]	~10^{10}–10^{12} Ω sq^{-1} [51]	~10^2–10^6 Ω s^{-1} [51,67]

Owing to its advantage of the electrochemical properties as mentioned above a vast development of biosensing applications has been recently discovered. Several proposals were established to use graphene-based electrodes for different platforms which could be used to immobilize biomolecules to create the best biosensing parameters. Since the graphene shows an enhancement of signal response due to its electrochemical response, various biosensing applications have been explored [69–71]. The high biocompatibility of graphene-based electrodes for different types of molecules especially glucose due to its high surface interaction area, electrical conductivity, and high electron transfer rate, makes a great advantage to develop more biosensors which can detect various types of molecules, as shown in Figure 4.

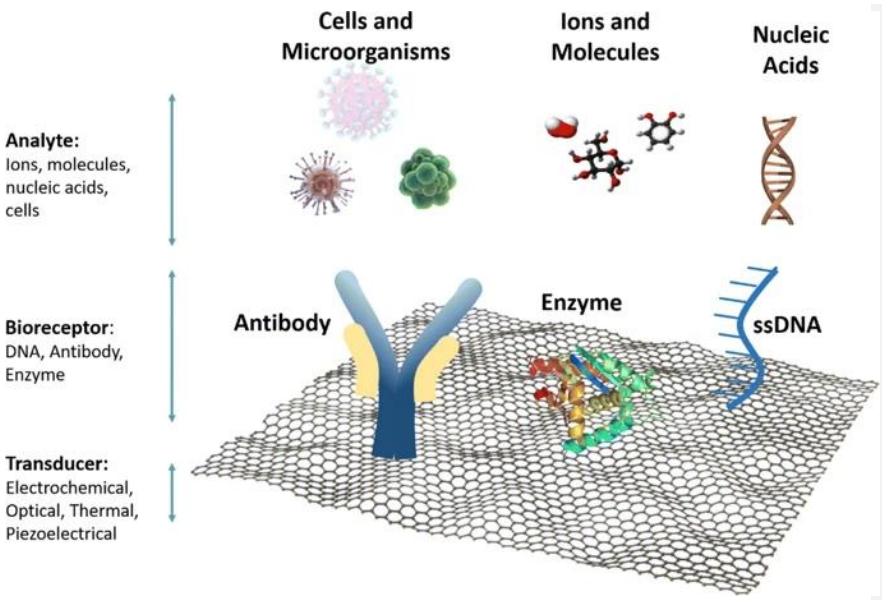

Figure 4. Schematic diagram of graphene-based biosensors for different biomolecules.

Considering the graphene-based electrodes biosensors, some aspects of electrochemical properties influencing the detection limit of the target need to be studied. Different compositions, synthesis methods, and synthesis batches of the graphene-based electrodes lead to different electrochemical properties such as selectivity, detection limit, and sensitivity of the biosensors. While the orientation of graphene and its diversity and bioreactors could be directly linked to the selectivity and sensitivity of the biosensors, the electrochemical sensing performance could be affected by the redox states of the electrode, and the type of the electrode compositions that leads to different interaction and detection limits of the molecule. Taking into account all of these properties and limitations, graphene-based electrodes for electrochemical biosensors (such as non-enzymatic glucose biosensors) are highly stable/sensitive due to their significant response time [72–78].

3. Mechanism of Cyclic Voltammetry Transducer

With consideration of all the advantages of the electrochemical properties of the graphene-based electrode, electrochemical biosensors have been developed widely. The non-enzymatic glucose sensor is defined as an electrochemical biosensor that uses its electrode as an electrocatalytic to measure glucose concentration [79]. Electrochemical detection principles lie behind the measurement for physicochemical properties of the bioreactor and target analyte to create a readable signal, such as electrical current, voltage, resistance, etc. If the chemical reaction between the target analyte and bioreactors (electrode) happens, the electrical properties of the solution changes due to the production of ion or electron [79,80]. In general, electrochemical detection techniques could be categorized as amperometric-based, impedimetric-based, potentiometric-based, or conductometric-based. An amperometric-based electrochemical biosensor is most widely used for the non-enzymatic glucose sensor [81–157].

Cyclic voltammetry (CV) is considered as an amperometric detection method [82]. While the electrocatalytic electrochemical properties of the electrode towards GOx could be characterized using the CV method, the redox potential based on the applied voltage at the working electrode surface could be analyzed [83,84]. In general, the cell contains three electrodes: Working electrode (WE—where the electrochemical action happens), reference electrode (RE—as a reference point to measure the potential for the other electrodes), and the counter electrode (CE—complete the circuit). A potentiostat is connected between WE and RE to apply a different potential. The integrated three electrodes of the CV cell work as the main components of the CV cell [85].

The applied voltage creates a potential for the chemical reaction at the electrode surface, where the reactance molecule moves to the electrode surface for mass interaction, then the electrode receives the chemical signal using the electron quantum tunneling concept (less than 2 nm of the electron tunneling distance) that leads to generating a current flow through the electrode that could be measured in a cyclic manner. This cyclic process gives information about the oxidation and reduction at the electrode surface using the following chemical equation [86,87]:

$$O + ne^- \rightleftharpoons R \tag{8}$$

Hence, the electrochemical reaction rate and redox potentials can be performed using single or multiple cycles. The graph of current vs. the applied voltage is called the cyclic voltammogram curve, where all the data of oxidation or reduction information is recorded at the working electrode [88]. Figure 5 shows a CV cell simulation and components with all the details of the electrical circuit scheme.

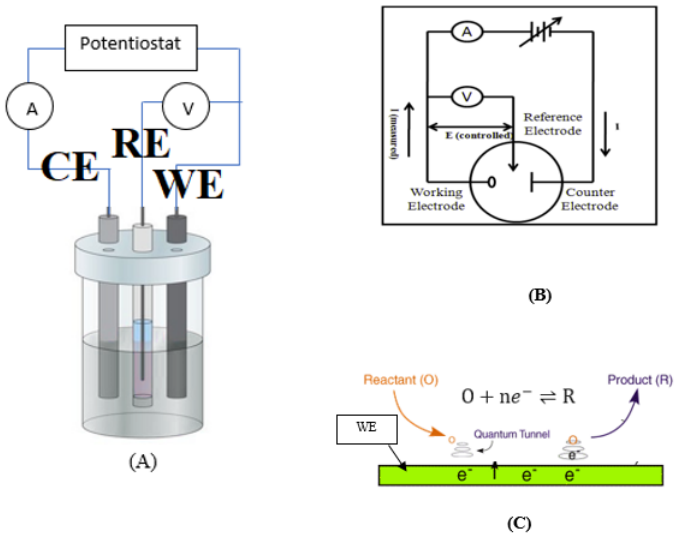

Figure 5. (**A**) A three-electrode cell with the utilization of cyclic voltammetry (CV) detection method—the input is the applied voltage while the output is the electrochemical analysis through the cyclic voltammogram

curve. (**B**) CV cell circuit—when the voltage applied to the electrochemical reaction starts on the electrode surface then the current starts to flow. (**C**) Simulation of electrode reaction with the reactant (glucose)—at a given applied voltage the reactant starts to move towards the electrode surface then the quantum tunneling happens to the electron, as a result, the reaction occurs to form the product.

Table 2 shows the main equations of the CV cell with the basic definitions. The oxidation and reduction at the graphene composites electrode surface could be understood using the Fermi-level energy (FE). When the applied voltage to the graphene electrode increases, the FE increases. As a result, the electron can jump from the electrode to the molecule due to being thermodynamically unfavorable where the process depends on the electron transfer rate, thanks to the electrochemical properties of graphene nanocomposites that make its electrodes very sensitive for different molecules with a very good electron mobility [86,88].

During the cyclic voltammogram process, the potential is swept up to a maximum value (oxidation) and then back down (reduction) again, which leads to a constant potential rate over time. The analytical GOx could use this technique as a fourth generation of the glucose nano-biosensor [89]. When the oxidation starts at the graphene nanocomposites electrode, the current starts to ramp up until it reaches the maximum value while the oxidation peak is the key observation [88]. The oxidation peak is proportional to the concentration of the glucose. If the reduction starts, the overall voltage starts to decrease, as a result, the overall current starts to decline—where the reduction peak will be present. Oxidation and reduction peaks are the key concepts of the voltammetry experiment [84]. Different scan rates lead to different results [82,89–91].

Table 2. Basic equations of the CV cell.

Equation	Definition
$I = \frac{dQ}{dt}$	Current = the change rate of the negative charge (electron) per time unit in the CV cell
$J = \frac{I}{A}$	Current density = the current flow through the unit area
$E = E^* - \frac{RT}{nF} \ln Qr$ E = Cell potential, E^* = Standard cell potential, Qr = Reaction Quotient = oxidized species/reduced species, n = number of electrons	The Nerst and Butler equation = gives information about the applied potential that controls the concentration of the oxidation and reduction species at the electrode surface and the rate of reaction
$\frac{I}{nFA} = K\left\{Coe^{-\alpha\theta} - Cre^{(1-\alpha)\theta}\right\}$ A = Electronic area, K = Heterogeneous Rate Constant, and $\theta = \frac{nF[E-\mathrm{E}*]}{RT}$	Butler-Volmer equation = gives a good relation between the current, potential, and concentration
$\varnothing = -ADo\left[\frac{\partial Co}{\partial x}\right]$ Do = Diffusion Coefficient of the reactance, x = the distance from the electrode	Fick's law = describes the diffusion of the reactance and product with respect to the distance from the electrode

Figure 6A shows the CV potential waveform. At t = 0 to t = 1—the potential increases and the overall current increases (oxidation). At t = 1 to t = 2—the potential decreases and the overall current decreases (reduction). During the reversible process at a given point, the current is fully determined according to the voltage. The peak potentials (Epa, Epc) and peak currents (Ipa, Ipc) of the anode (where the oxidation happens) and cathode (where the reduction happens) are extremely important as CV parameters, which lead to more information about the data of the glucose oxidation and reduction [83]. Figure 6B shows the cyclic voltammogram (current vs. voltage), this is the way that the current and the potential changes—swept from E1 to E2.

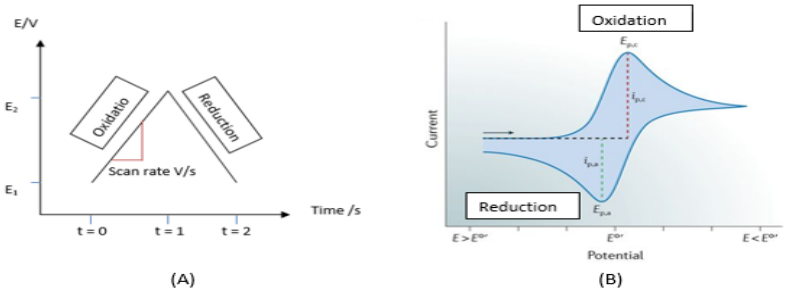

Figure 6. Cyclic voltammetry curves for detailed oxidation and reduction data. (**A**) Scan rate and GOx activity function with potential overtime. (**B**) The cyclic voltammogram.

The mathematical models of the CV analysis could be investigated for more understanding [83,87,92,93]. The peak current can be described mathematically through the following equation:

$$ip = 0.4463\, nFAC\left(\frac{nFvD}{RT}\right)^{1/2} \tag{9}$$

If the solution @ T = 25 °C, the peak current will be as follows:

$$ip = \left(2.69 \times 10^5\right) n^{3/2} A D^{1/2} v^{1/2} C \tag{10}$$

where,

i_p = current maximum in amps
n = number of electrons transferred in the redox event
A = electrode area in cm^2
F = Faraday Constant in C mol^{-1}
D = diffusion coefficient in cm^2/s
C = concentration in mol/cm^3
v = scan rate in V/s
R = Gas constant in J K^{-1} mol^{-1}, T = temperature in K

It is clear from the previous equation that the peak current depends on the scan rate, concentration, and diffusion of the electroactive species.

The midpoint between the oxidation and reduction peaks is given by:

$$E_{mid} = \frac{E_{p\ Cathodic} + E_{p\ Anodic}}{2} = E_0 + \frac{RT}{nF} \ln\left(\frac{D_r^{\frac{1}{2}}}{D_0^{\frac{1}{2}}}\right)^2 \tag{11}$$

where,

E_0 = redox potential
D_0 = Oxidation diffusion coefficient
D_r = Reduction diffusion coefficient

The capacitance can be approximately evaluated by the following mathematical expression:

$$C = \frac{Voltammetric\ Charge}{potential\ window \times Mass} \tag{12}$$

Hence, the voltammetric charge is defined as the sum of anodic and cathodic charges, then the specific capacitance can be written as:

$$C = \int_{E_1}^{E_2} \frac{i\,(E)dE}{2(E_2 - E_1)mv} \tag{13}$$

where,

C = Specific capacitance

$i(E)$ = Instantaneous current

$(E_2–E_1)$ = potential window width

m = mass deposited

Due to the current equation that addresses the relation between the voltage sweep and the current, the average capacitance can be understood through its mathematical definition:

$$I = \frac{dQ}{dt} = C\frac{dV}{dt} \tag{14}$$

$$C = I\frac{dt}{dV} \tag{15}$$

where,

I = faradaic current

dQ = change in charge

dV/dt = scan rate

The previous equation demonstrates the relationship between the capacitance, current flow, and scan rate. The fast scan rate generates low capacitance. The overall current and capacitance could be high due to the slow scan rate because the current has the time to flow.

The CV analysis is widely used in the non-enzymatic glucose biosensor to measure the electrochemical properties of the electrode towards GOx [81,94,95]. Luan V. H. et al. [96] successfully fabricated a silver nanowire (Ag NWs)/reduced graphene oxide (rGO) hybrid three-dimensional nanostructure as a working electrode for the ultra-sensitive non-enzymatic glucose sensor. The work is demonstrated at a scan rate of 100 mV/s, while the glucose concentration between 1 to 5 mM was tested in a 0.1 M NaOH solution. The Pt and Ag/AgCl worked as a CE and RE, respectively. While the cyclically applied voltage was between −0.1 to +0.7 V, the amperometric response was obtained at +0.5 V for the consecutive addition of 1 mM glucose in a 0.1 M NaOH solution. Figure 7 shows a scheme of the CV cell with the electrochemical characterization result.

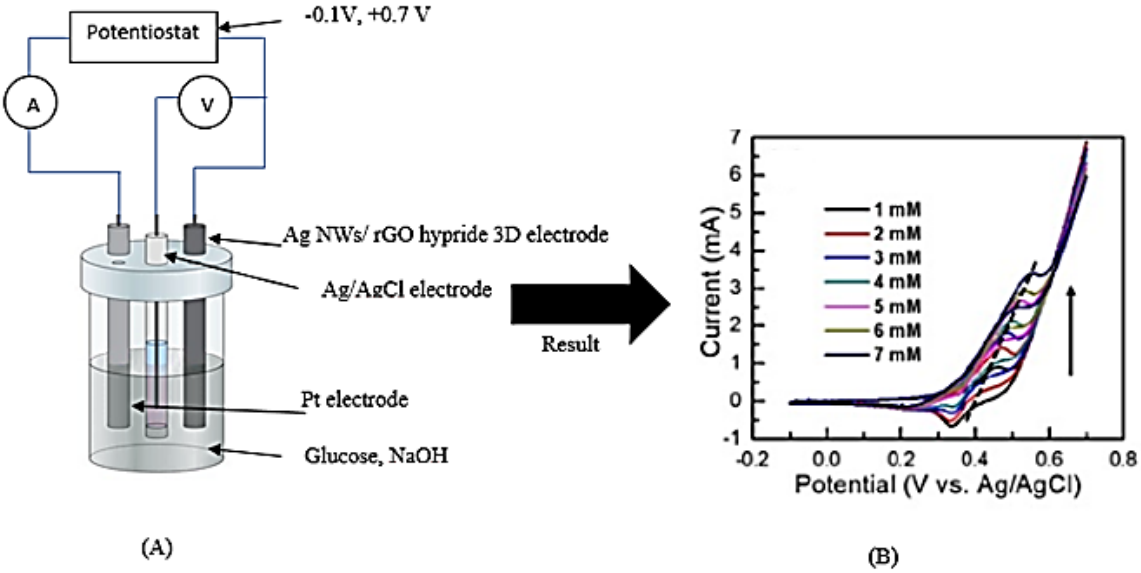

Figure 7. (**A**) The main component of the three-electrode CV cell utilized by Ag NWs/rGO hybrid three-dimensional (3D) electrode as a working electrode, Ag/AgCl as a reference electrode, and Pt electrode as a counter electrode, for glucose detection. (**B**) Results of the sensor with a full description of the oxidation peak and reduction peak at a scan rate of 100 mV/s.

Another example demonstrated by M. Sreejesh et al. [97] synthesized the composition of reduced graphene oxide (rGO)/zinc oxide (ZnO) for non-enzymatic glucose sensors. The group demonstrated the results using the CV technique. The modified glassy carbon electrode (GCE) with ZnO and rGO was used as a working electrode in a 1 M NaOH electrolyte, while the glucose is about 5 µM. The applied voltage was cycled between −0.8 and 0.8 V with a scan rate of 50 mV/s. The electrocatalytic reaction started when the peak was around −0.43 V. The electrochemical reaction could be understood from the following equation:

$$ZnO\ (OH) + Glucose \rightarrow Zn\ (OH)_2 + Glutonic\ Acide \quad (16)$$

$$Zn\ (OH)_2 + OH^- \rightarrow ZnO\ (OH) + H_2 + e \quad (17)$$

These examples can demonstrate that the oxidation and reduction peaks depend on the glucose concentration, diffusion, and scan rate exactly as we discussed previously.

4. Synthesis of Graphene and Its Derivatives

As the phenomenal electrochemical, physiochemical, and mechanical properties of graphene, GO, and rGO make it a superior material for electrochemical biosensors, the fabrication methods of the graphene which affect its characterization also influence the convenient advancement and performance of the electrochemical biosensors in terms of selectivity, sensitivity, and rapid cost-effective detection of the analyte [98–100]. Thus, the synthesis of graphene must take paramount considerations. On the one hand, it is vitally crucial to synthesize the controlled size (monolayer) and impurities-free graphene with restrained morphology to achieve structure-property compatibility. On the other hand, it is essential to design high yield, scalable, cost-effective industrial methods for their production [98,101].

For a clear explanation, the synthesis of graphene, GO, and rGO can be categorized into two main methods known as bottom-up and top-down. Every method has its own strategy. While epitaxial growth [102] (using thermal chemical vapor deposition strategy) and unzipping carbon nanotubes [103] are considered as top-down methods, the isolation [102] and (mechanically or chemically exfoliations) and reduction strategies [104–109] are considered as bottom-up methods as shown in Figure 8.

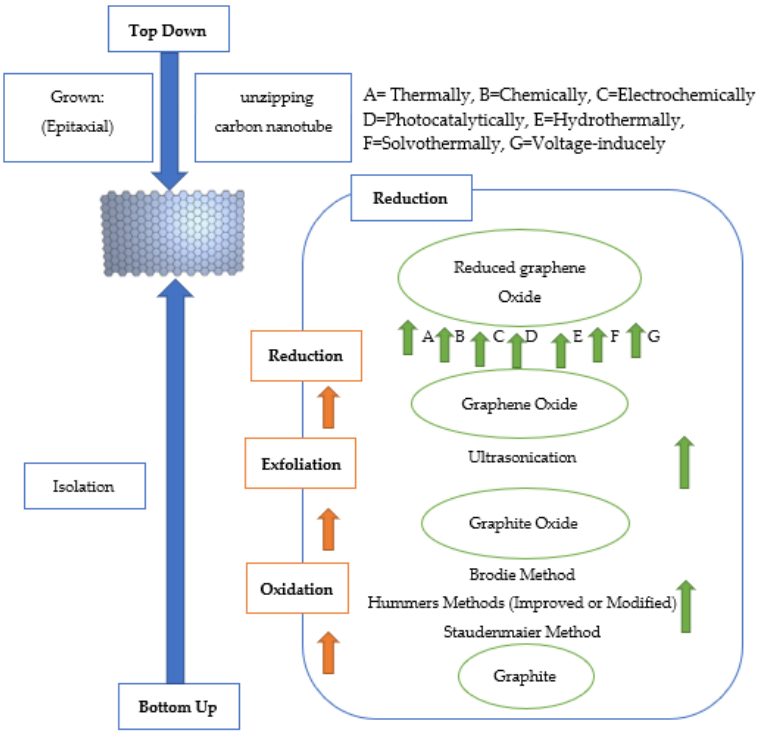

Figure 8. Bottom-up and top-down approaches for graphene, GO, and rGO synthesis methods.

The exfoliation method is originally based on isolation of a few layers from the bulk of graphene sheets by breaking the weak van dar Waals bonds and overcoming the attraction between adjacent layers. The number of mechanically and chemically approaches that depend on the exfoliation phenomena have exhibited promise for bulk and large-scale production [99,110]. The scotch tape technique is employed to peel atomically thin layers from a slab of HOPG flakes using adhesive tape to get individual crystal planes. Micromechanical cleavage is then applied by rubbing large crystal flakes against each other [99,111,112]. This method can obtain pristine structured graphene crystals without repeating defects in the structure of 2D graphene layers [99,110]. Although the mechanical exfoliation method provides a millimeter-sized graphene with electronic quality, their usage is restricted for biosensor applications because of the low yielding of mono-layer graphene sheets with a relatively high lateral dimension up to hundreds of micrometers besides the time consuming, making it only suitable for fundamental research and laboratories applications [98,99,101].

Liquid phase exfoliation (LPE) is another process of the same concept, it ordinarily includes dispersion of bulk graphite in an aqueous media, exfoliation, and purification. In principle through this concept, the presence of solvent applies external forces to overcome the interaction of van der Waal bonds as well as avoid substantial interruption of the plane of graphene. Thus, this method depends on the selection of optimum solvents that lower the interfacial tension between the solvent and graphene layer [113]. Recently, the usage of urea-based aqueous media shows greater capability superior to conventional toxic N-dimethylformamide (DMF)-based exfoliation [99,101,110]. Moreover, LPE can be improved by sonication, sheer mixing, or ball milling as well as by the addition of surfactants and intercalation with chemical species [101].

Sonication-assisted exfoliation via chemical wet dispersion involves the formation of shear forces and cavitation that act on the graphite bulk material and induce exfoliation followed by a solvent-graphene interaction that balance the interlayers attractive forces. However, this route involves the usage of high-boiling point solvents, e.g., N-methyl-pyrrolidone (NMP) and a long-time sonication, as well as, leads to the aggregation of graphene [113].

To circumvent graphene-sheet aggregation due to sonication, the surfactant-assisted liquid-phase exfoliation route is carried out using surfactants and biosurfactants as a dispersant and stabilizer that overcomes aggregation by steric and electrostatic repulsion. It involves reducing the high surface tension of water to be compatible with the hydrophobic graphene flakes by the separation of graphite into few-layered graphene flakes, which are coated with surfactant molecules [114].

In 2013, Ou et al. successfully validated the preparation of few-layered graphene dispersion from graphite powder, in a comparatively short-time sonication by combining liquid-phase exfoliation with heat-treatment attempts, which increase the interlayer surface of graphite and facilitate the access of organic molecules to graphite lattice. The pristine graphene was heat-treated in (NMP) and stabilized by adding polyvinyl pyrrolidone (PVP), which leads to the formation of a well-dispersed few-layered flakes by sonication for up to 20 h [114,115].

Moreover, Gomez et al. demonstrated in 2019 a novel approach to produce stable and well-dispersed few-layered graphene dispersion by the exfoliation of hydrothermally expanded graphite through sonication for 3 h and centrifugation. The selected cationic surfactant, hexadecyltrimethylammoniumbromide (CTAB), is a precursor for constructing graphene nanocomposites, which are utilized in promising electrochemical sensors and biosensors. The concentration of the graphene dispersion ranged from 40 to 60 μg mL^{-1}, as well as, presented lower (edge/basal) defects of few-layered graphene, up to five layers [114].

Recently, the solution-based chemical exfoliation of graphite is the most promising approach for the construction of biosensor devices including electrochemical biosensors due to its large scale and facile technique besides low cost and high-quality production [98,99]. Graphene derivatives (GO, rGO) can be produced from graphite by chemical oxidation. For instance, Hummer's method is used to produce graphite oxide. In this method, potassium permanganate is added to a mixture of graphite, sodium nitrate, and concentrated sulfuric acid. During oxidation, small ions embed to bulk graphite oxide and weaken the interaction between the layers. Sonication grants exfoliate GO flakes from

graphite oxide sheets and produce a reduced graphene oxide consecutive reduction that can be utilized to enhance electrical properties [99].

In addition, the electrochemical liquid-phase exfoliation of graphite is a method that involves applying an electric current, where commonly HOPG is used as a working electrode in liquid electrolytes such as ammonium sulfate. It has been considered that the electrochemical potential leads to sufficient ion intercalations between graphene flakes to break van der Waals forces and expand their interlayer spacing. Subsequently, gas eruption expands the graphite and results in its exfoliation. Then, flaked-off graphene sheets are collected by vacuum filtration and dispersed in organic solvents such as (DMF) [101,116]. Radical species that are generated by electrolysis of water and ruin the graphene yield can be reduced by the usage of radical scavengers. The electrochemical exfoliation method is advantageous because of the high yield (75% of one layer and few layers with a lateral scale, 5–10 μm) besides the stability of the dispersible yield for several weeks without precipitation. Moreover, the fabricated graphene sheets exhibit high quality features with minimum defects, high C:O ratios of ~25.3, and electronic mobility values of 405 cm^2 V^{-1} S^{-1}. Furthermore, the production rates can be increased by utilization of a dual graphite electrode (cathode and anode) and applying an alternating current [101]. In situ functionalization of graphene can be induced during the electrochemical exfoliation to give variant graphene-based composite materials [116].

The copper-oxide graphene composite was synthesized by electrochemical exfoliation and used for the fabrication of a functionalized non-enzymatic glucose biosensor. Mono-layered graphene flakes were synthesized by this method, in which graphite electrode acts as the anode and platinum electrode acts as the cathode. The electrochemical biosensor fabricated using the CuO-rGO composite exhibited potential advances such as high selective response towards glucose in the presence of other interrupting species, high sensitivity of 2182 μA mM^{-1} cm^{-1}, and better linear response up to 22 mM [117]. Paramasivam Balasubramanian et al. [118] introduced very desirable glucose detection results using modified electrode-based copper nanoparticles that decorated reduced graphene oxide ERGO/CuNPs using the modified Hummer's method for GO preparation, followed by an electrochemical reduction for rGO preparation. However, the electrodeposition method was highly desired to deposit the copper nanoparticles for electrode modification.

Unzipping/opening of the CNTs process for graphene fabrication can be attributed under the top-down approach. It can be achieved by a solution-based oxidative treatment with an oxidizing agent such as hypermanganate as well as through the way of plasma etching of multi-walled CNTs (MWCNTs) with PMMA films to produce graphene nanoribbons [41,101,119,120]. In this method, the utilization of the produced graphene from MWCNTs is restricted in the electrochemical applications due to the presence of intercalated metallic impurities that alter the electrochemical properties of graphene as well as toxicity [119].

Graphene can be epitaxially grown on electrically insulating surfaces such as silicon wafers through withdrawal of Si atoms from silicon carbide (SiC) and consequent graphitization of the carbon atoms, depending on the high-annealing temperature and the ultrahigh vacuum. The produced graphene sheet exhibits a variable charge carrier mobility depending on the substrate face on which the graphene sheets are grown. The carrier mobility ranges of the graphene sheet on Si-terminated face and C-terminated face are 500–2000 and 10,000–30,000 cm^2 V^{-1} S^{-1}, respectively [120]. The Georgia Tech team developed a confinement-controlled sublimation (CCS) process which involves the enclosure of graphite with the SiC growth crystals, thus, segregating the evaporated silicon and enhancing the equilibrium process. This (CCS) method leads to the production of nano-patterned graphene structures with high mobility on both surfaces of the SiC substrate [121].

The epitaxial graphene (EG) is mainly applicable for laboratory studies and slot applications, such as high-frequency transistors due to the dependence on the high temperature, limitation of EG size with the size of wafers in the technique, as well as the high cost of silicon carbide wafers [120]. In general, both strategies, unzipping CNTs and epitaxial growth on SiC, require the involvement of

high temperature and vacuum conditions, expensive gases, highly defined microfabrication devices, thus, hampering the utilization in a large industrial scale [121].

Chemical vapor deposition (CVD) has been sighted as the most up-and-coming approach to growing large-scale graphene films with a high quality. The graphene sheets are assembled by the thermal decomposition of hydrocarbons, such as methane, and the self-organization of the composed carbon atoms on transition metal substrates, mostly Cu and Ni, followed by segregation of the graphite layer on a metal substrate through CVD [122–125]. Among the various transition metals used, the copper substrate is ideal to produce a single layer of graphene sheets with high electrical properties due to its controlled catalytic activity and low solubility of the formed carbons; however, the crystalline nickel substrate is still used in this method but it is challenging to provide monolayer films with adequate electrochemical properties [99,101].

In this method, as presented in Figure 9, hydrogen gas is mixed with methane during the growth to eliminate the undesired impurities of carbon. The formed graphene monolayer is transferred to another substrate. Due to the tight bond between the carbon and copper substrate, the graphene films are covered with a protective polymethylmethacrylate (PMMA) using a technique called spin coating, then the copper substrate is etched away with $FeCl_3$.

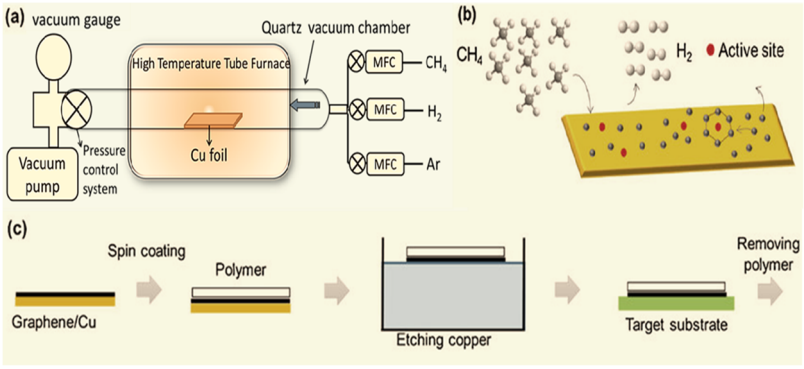

Figure 9. Graphene synthesis via chemical vapor deposition (CVD): (**a**) Chemical vapor deposition reactor. (**b**) Growth mechanism of graphene on the copper substrate via deposition. (**c**) Schematic illustration of the transfer process of the graphene sheet; spin coating with a polymethylmethacrylate (PMMA) polymer, etching copper with $FeCl_3$, graphene on a PMMA support is transferred onto the Si/SiO_2 target substrate, and PMMA is removed by acetone.

To proceed, the graphene on a polymer support is transferred onto the Si/SiO_2 substrate and PMMA is polished with acetone. In addition, CVD graphene films commonly acquire defects during formation due to the subsequent merging of multiple-crystalline domains and the formation of grain boundaries, which hinder the mechanical and electronic properties of graphene. Thus, several approaches occurred including the addition of surface oxygen to graphene and the predefined orientation on a single-crystalline Ge substrate [101,125]. Earlier, chemical vapor compositions (CVD) were introduced to produce a 3D graphene-cobalt oxide electrode for glucose detection. The group used a sample hydrothermal process in which the cobalt oxide nanowire grows up on a 3D graphene foam prepared by CVD [126]. In comparison with the exfoliation methods, chemical vapor deposition can synthesize larger graphene films with high mobility up to 10^5 cm^2 V^{-1} S^{-1}; however, the structural defects or corruptions that originated during the etching and transfer process possess limiting factors for high-performance graphene-based electronic and optoelectronic sensors [99,101].

In addition to the previous top-down methods, 2D nano-graphene materials can be synthesized by wet chemistry methods, which are advantageous in low cost, scalable high yield, and uncontaminating. This method is used to prepare MoS_2 nanoplates, which are disorganized graphene-like sheets with about 30 nm thickness, by the introduction of $Mo(O)_6$ and S as a precursor in the one-step hydrothermal reaction as well as used to synthesize flower such as MoS_2 nanostructures by the usage of MoO_3

nanorodes as a precursor in the two-step hydrothermal method. However, it is still challengeable to control the size and thickness of 2D nanomaterials by chemical synthesis methods [127].

In recent years, the functionalization of graphene has gained significant attention due to the sensitivity of graphene to a reproducible, effective, and homogenous functionalization in comparison with other carbon materials; thus, enhancing its sensing capabilities for different electroanalytical applications [100,128]. Numerous modification techniques have been utilized to incorporate biorecognition molecules in graphene that are capable of finely detecting the target biomolecules and improving the dispersion of graphene. Two major functionalization methods are the peer-reviewed covalent and noncovalent functionalization [110].

Covalent functionalization is formed on sp^2-hybridized carbon atoms of the π-conjugated crystal which alter the electronic characterization and physical structure. The grafting of molecules can occur either at the edges and/or on the basal plane by two methods of heteroatom doping and by a reaction with the unsaturated double bond of graphene [128,129]. Graphene is very stable thermally and chemically, thus, the covalent functionalization method needs high energy procedures and is established by converting sp^2 π-conjugation into sp^3. The rehybridization of one or more carbon atoms by condensation, addition, nucleophilic substitution, and electrophilic addition reactions leads to the installation of scattering sites in graphene [128].

Several functional groups such as alkyl, amino, and hydroxyl groups can be covalently bonded onto graphene, where it acts as chemical switches to introduce other functional molecules such as polymers. In addition, this method has a control on the carrier density and bandgap engineering according to the type of the added functional groups and the degree of functionalization. For instance, the binding of acceptor functional groups or donor functional groups gives rise to the p-type semiconductor and an n-type semiconductor, respectively [128].

In contrast to the covalent functionalization method, the noncovalent approach is achieved through dispersion and electrostatic forces, van der Waals, and hydrophilic and hydrophobic interactions, which do not affect the intrinsic and electronic properties of graphene but can adjust the morphology while providing new chemical groups on the graphene structure [128,129]. In this method, surface functionalization with various molecules is achieved in several ways, such as surfactant adsorption, wrapping of polymers as well as interaction with biomolecules and metal nanoparticles. For instance, noncovalent functionalization of graphene with nanoparticles and nanowires is used in non-enzymatic glucose sensing with remarkable detection limits [128].

In brief, several reduction strategies are used for the synthesis of rGO, through three main simultaneous procedures: (1) Oxidation methods, (2) exfoliation techniques, (3) reduction process. The oxidation methods, Brodie, Staudenmaier, and Hummer's (improved or modified) methods, produce graphite oxide from bulk graphite. Recently, the modified Hummer's method is mainly used, considering the low reaction time (<3 h), while the other mentioned methods take up to (12 h) or several days. Consequently, the exfoliation by ultrasonication is carried and then followed by reduction strategies including (a) thermally, (b) chemically, (c) electrochemically, (d) photocatalytically, (e) hydrothermally, (f) solvothermally, (g) voltage-inducely as well as microwave irradiation methods [98].

Moreover, the hydrothermal method is a simple strategy for the reduction of graphite oxide to rGO, where the degree of the reduction is dependent on the reaction temperature due to the effect of temperature on the interlayer distance, thus, as the temperature increases the reduction of graphite oxide increases to synthesize more rGO. The solvothermal process is advantageous because of the high yield, relatively low C:O ratio, and mild synthesis conditions as well as the produced graphene-like sheet that exhibit highly resistive properties, considering the high amount of residual functional groups that are produced; however, the produced yield expressed irreversible defects, besides an ample number of oxygen-containing functional groups [130]. For instance, Sang et al. used the hydrothermal method for the fabrication of reduced graphene oxide/CuO, which is utilized in non-enzymatic glucose sensors. In 2017, a novel ultrasensitive non-enzymatic glucose sensor was fabricated by an in situ

layered 3D CuS/RGO/CuS nanocomposite on Cu foam by the one-step hydrotherm-assisted process. The electrochemical properties of the produced composite, CuS/RGO/CuS/Cu, was evaluated by cyclic voltammetry and amperometry techniques and utilized as an electrode regarding its high sensitivity of 26.66 μA mM^{-1} cm^{-2} to glucose sensing and low detection limit of 0.5 μm [131].

Furthermore, the microwave irradiation method is a novel approach for speeding up the synthesis of graphene and enhancing the quality of the yield. The principle of this method is the utilization of high-frequency wave on graphite or other carbon materials, which lead to the speed elevation of their temperature, through dipolar polarization and ionic condition. During the irradiation of the sample, the dipolar or ions molecules are sensorial to the electric field, which lead to their rotation and friction, subsequently, increasing the temperature of the sample. This method is used for the fabrication of various graphene structures, such as the 3D graphene-nanotube-nickel nanostructure by the dispersion of the GO powder and nickelocene in acetonitrile (CH_3CN) and irradiation of the dispersion mixture at 700 W for 5 min as well as boron and nitrogen co-doped rGO by the dispersion of GO in a solution of boric acid and ammonia, followed by 6 h of stirring and 80 °C drying temperature, then the usage of an irradiation at 700 W for 4 s [132].

In addition, the microwave irradiation method has been used as an approach for efficient improvement of the liquid-phase exfoliated graphene and reduced graphene oxide by the reduction of oxygen content and the limitation of structural defects, thus, enhancing the charge-carrier mobilities. In the case of LPE, graphite is exfoliated in molecularly engineered ionic liquids by irradiation at 30 W, leading to the production of a high-yield mono-layer structure (>90%) and the enhancement of affinity. The high quality reduced graphene oxide is produced by strong microwave short pulses at 1000 W for 1 or 2 s, leading to the reduction of the lattice defectives, besides the microwave-rGO exhibits significantly high charge-carrier mobilities (1500 cm^2 V^{-1} S^{-1}), which is higher than that of rGO and LPE. Nevertheless, this method is limited, because the used reactors restrain the industrial cost-effective scale-up of this strategy [101].

5. Graphene-Based Electrode for Non-Enzymatic Glucose Biosensor

The emerging nanomaterials-based graphene composition with a non-enzymatic glucose sensor would meet the scientific demands such as cost effectiveness, synthesis approach, biocompatibility, stability, electron-transfer kinetics, and sensitivity [17,32,33,133,134]. The superlative properties of graphene nanosheets make them a preferable material for developing hybrid nanostructures, which add synergistic features to the sensor, especially, non-enzymatic glucose biosensors [135]. In recent years, various metals, such as platinum (Pt), gold (Au), palladium (Pd), nickel (Ni), and copper (Cu) as well as metal oxides such as Cu_2O, RuO_2, NiO, Co_3O_4, and MnO_2 were employed to modify non-enzymatic glucose electrodes [136,137].

Recently, three-dimensional (3D) electrodes have been employed in the fabrication of non-enzymatic glucose biosensors to enhance the performance by widening the specific surface area. Mazaheri et al. [135] utilized for the first-time hybrid electrodes based on rGO/Ni/ZnO arrays for non-enzymatic biosensing. They have studied the effect of rGO nanosheets on the electrical activity of Ni/ZnO heterostructure. It is shown that the integration of rGO, Ni, and ZnO nanorods exhibit better performance in the electrochemical properties of the biosensor. While Ni/ZnO prisms have a linear range (1–8.1 mM), a sensitivity of 824.34 μA mM^{-1} cm^{-2}, and a detection limit (0.28 μM), the utilization of reduced graphene oxide adds advantages of higher sensitivity of 2030 μA mM^{-1} cm^{-2} and lower detection limit (0.15 μM).

Mahmoud A. Sakr et al. [138] developed a performance-enhanced (enhanced selectivity and sensitivity) non-enzymatic glucose sensor based on graphene-heterostructure. The proposed sensor is a composite of graphene (G)/platinum oxide (PtO)/n-silicon (Si) heterostructure. While the atomic layer deposition (ALD) was used to deposit the PtO thin film in a N-type silicon wafer at 275 °C for 50–500 ALD-cfycles, the bottom-up approach was used to produce graphene using the Plasma Enhanced Chemical Vapor Deposition (PECVD) at a pressure of 1500 m Torr and 600 °C. The group

studied the effect of the PtO thickness on the catalytic activities which played a significant role in the sensitivity and selectivity. Increasing the PtO layer thickness leads to enhancing the sensitivity by 150% to reach up to 30 μA/mM.cm^2.

Zongxu Shen et al. [139] proposed a non-enzymatic glucose sensor based on a nickel nanoparticle–attapulgite-reduced graphene oxide-modified glassy carbon electrode. The NiNPs/ATP/RGO-GCE electrocatalysis towards the GO_x was measured by cyclic voltammetry and amperometric. The group tested the CVs of NiPs/ATP/RGO-GCE in 0.1 M of NaOH at different scan rates of about 0.020.1 $V\ S^{-1}$. Moreover, they investigated the CVs of NiNPs/ATP/RGO-GCE in 0.1 M of NaOH at a different glucose concentration of about 0–3 mM. Furthermore, the electrochemical performance of GCE, NiNPs/RGO-GCE, and NiNPs/ATP/RGO-GCE was investigated in 0.1 M NaOH at the absence (1; 3; 5) and presence (2; 4; 6) of the glucose. The anodic/cathodic potential peaks of GC, NiNPs/RGO-modified, and NiNPs/ATP/RGO-modified electrodes were investigated as 0.322/0.488, 0.292/0.403, and 0.319/0.458 V, respectively. The group demonstrated a sensitive sensor in the real glucose samples of 1414.4 $\mu A\ mM^{-1}\ cm^{-2}$, linear range (1–710 μM), and detection limit (0.37 μM).

Dong et al. [126] reported a composite material of 3D graphene-Co_3O_4 nanowires as a freestanding electrode for non-enzymatic glucose sensing. The biosensor achieved a sensitivity of 3.39 mA mM^{-1} cm^{-2} and a LOD of 25 nM, which are nearly six times higher and two times lower than those of the CoO NRs-modified electrode in Kung's study. However, the up to 80 mM linear range of the 3D graphene/Co_3O_4 nanowire electrode is much smaller than those of both Ding's and Kung's biosensors. The biosensor showed a capability for glucose detection in micro-droplets within the linear concentration range of 50–300 mM.

S. Darvishi et al. [140] used an Ni nanoparticle-decorated reduced graphene oxide (Ni-NPs/rGO) to detect the glucose. The electrode has shown excellent electrochemical properties for GOx with a linear range of 0.25–1200 μM and a detection limit of 0.01 μM. Li Wang et al. [141] demonstrated a green strategy for producing a graphene foam-like 3D porous carbon/NiNPs nanocomposites-based glucose detection electrode. The team used a 3D porous carbon derived from the waste biomass to produce a highly sensitive biosensor. The sensor shows a linear range of 15.84–6.48 mM, and a detection limit of 4.8 μM. Wei Lv et al. [142] prepared a DNA-dispersed graphene/NiO hybrid material deposited in a glassy carbon electrode using a self-assembly process to prepare the GNS/NiO powder while ssDNA was employed to produce the GNS/NiO/DNA hybrids. The experimental work shows low detection limits and good sensitivity. Baiqing Yuan et al. [143] fabricated a graphene oxide/nickel oxide modified glassy carbon electrode (NiONPs)/GO/glassy carbon (GC)-based non-enzymatic sensor. The work was characterized by the scanning electron microscope (SEM), electrochemical impedance spectroscopy (EIS), and cyclic voltammetry (CV). NiONPs were synthesized on the surface of GO electrochemically. The NiONPs/GO/GC electrode shows a good electrocatalytic behavior towards GOx with a linear range of 3.13–3.05 mM and a limit of detection of 1 μM. Palaniappan Subramanian et al. [144] designed graphene oxide–Ni $(OH)_2$ composites-based electrodes for non-enzymatic glucose sensing. The rGO/Ni $(OH)_2$ shows the linear range of 15–30 mM with a good sensitivity. The electrophoretic deposition has been used for sensing matrix fabrication, while the matrix characterization was through X-ray photoelectron spectroscopy, Raman spectroscopy, and cyclic voltammetry. Luan H.V. et al. [96] demonstrated a successful use of a silver nanowire/graphene hybrid three-dimensional (Ag NW/RGO hybrid 3D) nanostructure for an ultra-sensitive non-enzymatic glucose sensor. While the microwave method followed by oxidation and exfoliation of an expanded graphite was used to prepare the GO, the hydrothermal reduction of silver salt was used for the Ag-NWs preparation. The hydrothermal sol-gel method was used for the Ag NW/RGO hybrid 3D preparation. The material characterization was obtained using X-ray diffraction (XRD) measurement, ultraviolet-visible (UV–Vis) spectroscopy, and scanning electron microscopy (SEM). The electrochemical properties were obtained using the CV method to check the electrocatalytic activity of the electrode towards the GOx. The sensor investigated a very high sensitivity of about 1249.1 μA mM^{-1} cm^{-2}, and a low LOD of about 0.38 μM. Figure 10 describes the electrocatalytic activity of this sensor.

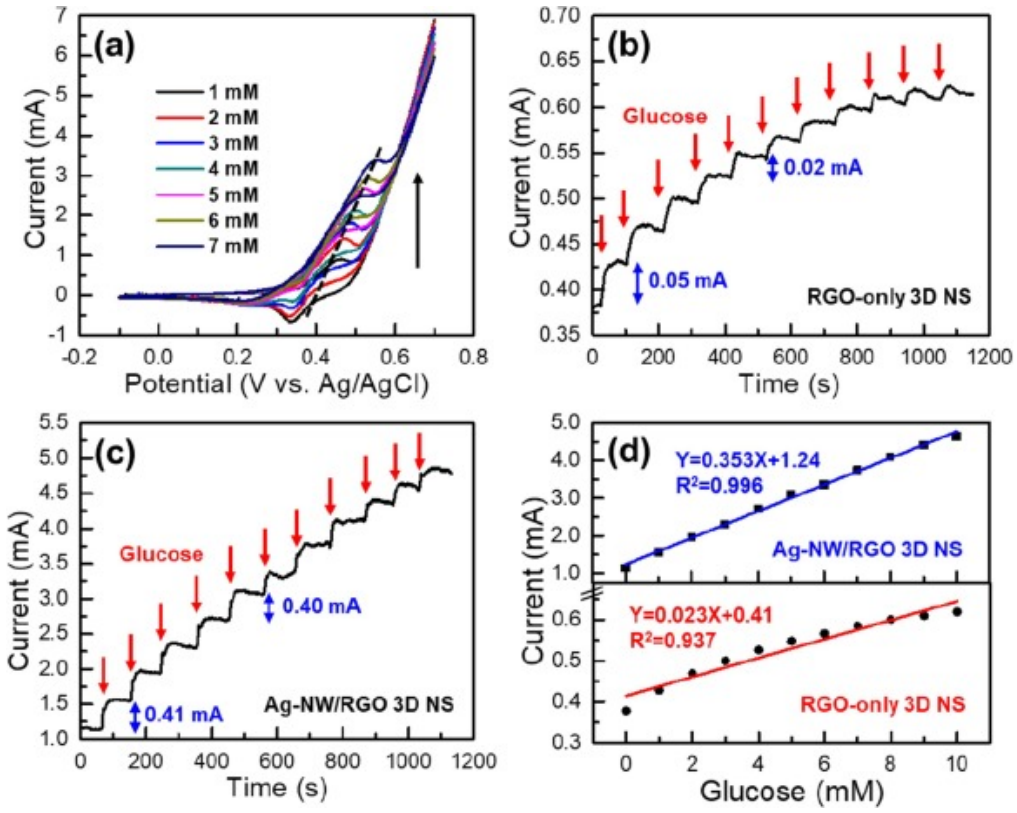

Figure 10. (**a**) The CV response of the Ag-NW/RGO hybrid 3D towards glucose oxidation at different concentrations of glucose. (**b**) The amperometric responses of rGO-only 3D NS for comparison. (**c**) The Ag-NW/RGO hybrid 3D NSs amperometric response at each additional 1 mM of glucose. (**d**) The linearity detection between the glucose concentration and current for rGO-only 3D NS and Ag-NW/RGO hybrid 3D NSs. Source: https://www.sciencedirect.com/science/article/pii/S221137971931040X#s0035.

Beibei Zhan et al. [145] employed an Ni $(OH)_2$/3D graphene foam for nonenzymatic glucose detection. The hydrothermal process has been used to deposit the hexagonal Ni $(OH)_2$ nanosheets on the surface of 3DGF while the 3DGF used a chemical vapor deposition-growth process. The Ni $(OH)_2$/3D graphene foam was characterized by scanning electron microscopy (SEM), transmission electron microscope (TEM), Raman spectroscopy, and X-ray diffraction (XRD). The work has been demonstrated by a linear range of 1–1.17 mM and a detection limit of 0.34 µM.

Amin et al. [146] successfully made a non-enzymatic sensor based on a $NiCo_2S_4$/rGO nanocomposite, this kind of sensor shows a good redox tenability and good charge transport property. While the applied potential was +0.35 V, a wide linear range was recorded as 1–4.0 mM, sensitivity of 18.89 mA mM^{-1} cm^{-2}, and detection limit of 0.65 µM. Similar work was prepared by Akhtar MA et al. [147], the article shows a functionalized graphene oxide (fGO) decorated with magnetite (Fe_3O_4) nanoparticles and PANI for the non-enzymatic glucose sensor. The electrochemical properties of a fGO-Fe_3O_4-PANI nanocomposite were measured using CV techniques. The fGO-Fe_3O_4-PANI nanocomposite modified electrode shows a very good oxidation result towards glucose with a linear range of 0.05–5 mM and a limit of detection 0.01 µM by taking advantage of the improvement of the electrocatalytic activity of N-doped graphene [148]. Foroughi et al. [149] demonstrated a nitrogen-doped graphene non-enzymatic glucose sensor which detects a biological PH value. The team shows a limit of detection of 0.13 µM, sensitivity of 774.23 µA mM^{-1} cm^{-2}, and linear range of glucose concentration 0.13 –14 mM @ pH 13, while a superior sensitivity of 122.336 µA mM^{-1} cm^{-2}, the detection limit of 14.52 µM, and fast linear range of 14.52 –10 mM @ biological pH (7.4) value. Yang et al. [150] successfully fabricated a non-enzymatic glucose detection using the nanoneedle-like copper oxide on an N-doped reduced graphene oxide. The constructed sensor demonstrates an increasing contacting area between the

electrode and electrolyte. The result investigated a linear range of 0.5–639 µM and a low detection limit of 0.01 µM. Graphene with Ni_2P nanoparticles could be used for glucose detection.

Zhang et al. [151] showed the enhancement of the electrochemical properties of the non-enzymatic glucous sensor using porous Ni_2P/graphene composites. This metal-organic framework shows a very good electrocatalytic activity towards glucose electrooxidation. The work was characterized by scanning electron microscopy (SEM), high-resolution transmission electron microscopy (HRTEM), transmission electron microscopy (TEM), powder X-ray diffraction (PXRD), and X-ray photoelectron spectroscopy (XPS), while the electrochemical properties were characterized by cyclic voltammetry (CV) and amperometric. The Ni-MOF-74 nanocrystals were prepared using PVP as a stabilizer while the Ni_2P/G composite structure was obtained using sodium hypophosphite. The sensor shows a linear range between 5–1.4 mM with a detection limit of 0.44 µM. Khosroshahi et al. [152] created a non-enzymatic sensor for glucose detection in the human serum based on a three-dimensional graphene foam decorated with Cu-$x$$Cu_2O$ nanoparticles. The electrochemical properties of Cu-based nanoparticle concentrations were measured using cyclic voltammetry, electrochemical impedance spectroscopy, and differential pulse voltammetry. The Cu–Cu_2O NPs@3DG foam shows a linear range of 0.8–10 mM, a high sensitivity of 230.86 µA mM^{-1} cm^{-2}, and a detection limit of 16 µM. The sensor shows a new way for the inexpensive non-enzymatic glucose sensor.

More work in graphene-based electrodes for non-enzymatic glucose sensors have been summarized, as shown in Table 3. The table reviews the metal/graphene composites in non-enzymatic glucose sensors such as Au/GO, Pd/GO, Pt/GO, etc. Moreover, the table demonstrates metal oxides/graphene composites in non-enzymatic glucose sensors such as (Cu(OH)2/, Cu2O, CuO, NiO)/(graphene composites), etc. Furthermore, alloy/bimetallic/hybrid metal/graphene composites and nanoparticles/polymer/graphene composites have been introduced. The sensitivity, limit of detection, linearity, principle detection, and sample types of glucose have been summarized for a big comparison picture to demonstrate the electrochemical properties for each sensor.

Table 3. Graphene-based electrodes for non-enzymatic glucose sensors.

Electrode Modification	Linear Range	LOD	Sensitivity $mA\ mM^{-1}cm^{-2}$	Principle	Sample	Ref
GCE/$NiCo_2$ O_4/N-rGO/IL	0.001–4.555 mM @ +0.5 V potential	0.18 µM	3.76 mA mM^{-1} cm^{-2}	CV	Real human blood serum	[81]
GCE/($Ni(OH)_2$/N-rGO	0. 5–0.0115 mM @ +0.45 V potential	0.12 µM	3.214 mA mM^{-1} cm^{-2}	CV and amperometry	Real human blood serum	[153]
GCE/Ni-MoS_2/rGO	0.005–8.2 mM @ +0.575 V 0.55 potential	2.7 µM	0.2566 mA mM^{-1} cm^{-2}	CV and amperometry	Purchased glucose	[154]
$CuCo_2O_4$/Porous GO	0.5–3.354 mM @ 0.55 V	0.15 µM	2426 µM mM^{-1} cm^{-2}	Amperometry CV	Human serum	[155]
Disposable CuNCs-DLEG	25–4.5 mM @ 0.55	0.25 µM	4532.2 µM mM^{-1} cm^{-2}	Amperometry/CV	N/A	[156]
LSC/rGO/GCE	2–3350 µM @ 0.6	0,063 µM	330 µM mM^{-1} cm^{-2}	Amperometry	N/A	[157]
PDDA-graphene/CuO	0.4–4 mM @ 0.58	0.20 µM	4982.2 µM mM^{-1} cm^{-2}	Amperometry CV	Human blood serum	[158]
Nafion/CuNWs-MOFs-GO/GE	20–26.6 mM @ 0.3 V	7 µM	7.72 µM mM^{-1} cm^{-2}	Amperometry CV	Human serum, beverages	[159]
Cu NPs@rGO	1–2 mM	0.34 µM	150 µM mM^{-1} cm^{-2}	DPV/CV	Human blood serum	[160]
Ni_2P/G/GCE	5–1.4 mM @ 0.6 V	0.44 µM	7234 µM mM^{-1} cm^{-2}	Amperometry CV	Human serum	[151]
$CoNi_2Se_4$-rGO@Ni foam	1–4 mM @ 0.35	0.65 µM	18,890 µM mM^{-1} cm^{-2}	Amperometry CV	Human blood	[146]
Pt/Ni@ rGO	0.02–5 mM @ 0.5 V	6.3 µM	171.92 µM mM^{-1} cm^{-2}	Amperometry CV	Commercial beverages	[161]
$Co(OH)_2$NPs/3DGF/GCE	2–1.4 mM @ 0.45 V	0.67 µM	2410 µM mM^{-1} cm^{-2}	Amperometry	Human urine, human blood serum, fetal calf serum	[162]
Au-rGO/PU WSNF	1–1 mM	500 nM	140 µM mM^{-1} cm^{-2}	CV Amperometry	Human sweat	[163]

Table 3. *Cont.*

Electrode Modification	Linear Range	LOD	Sensitivity $mA\ mM^{-1}cm^{-2}$	Principle	Sample	Ref
Au/Thi/GO/GCE	0.0002–0.002, 0.002–0.022 mM	0.05 µM	N/A	CV and amperometry	N/A	[164]
Au/BSA/rGO/GCE	0.02–1.6, 1.6–16.6 mM @ 0 V	5 µM	11.5 µA mM^{-1} cm^{-2}, 3.8 µA mM^{-1} cm^{-2}	CV and amperometry	Human serum	[165]
Pd/GO/GCE	0.2–1.6 mM @ 0.4 V	N/A	N/A	CV and amperometry	Purchased glucose	[166]
IL/$SCCO_2$/Au/graphene/GC	N/A @ 0.3 V	0.062 µM	97.8 µA mM^{-1} cm^{-2}	CV and amperometry	Human serum	[167]
Pt/GO/GCE	0.002–10.3, 10.3–20.3 mM @ 0.47 V	2 µM	1.26 µA mM^{-1} cm^{-2}, 0.64 µA mM^{-1} cm^{-2}	CV and amperometry	Purchased glucose	[168]
Au/GONR/CS	0.005–4.92, 4.92–10 mM @ 0.2 V	5 µM	59.1, 31.4 µA mM^{-1} cm^{-2}	amperometry and linear sweep voltammetry	Purchased glucose	[169]
Au/GA/GCE	0.01–16 mM	4 µM	N/A	CV	Purchased glucose	[170]
Ag/GO/GCE	1–14 mM @ 0.6 V	4 µM	11 µA mM^{-1} μg^{-1} cm^{-2}	CV and amperometry	Human blood	[171]
Pt/GOH	5–20 mM @ 0.1 V	N/A	137.4 µA mM^{-1} cm^{-2}	CV and amperometry	Real blood	[172]
Au/graphene/GCE	0.1–2.0, 2.0–16 mM @ 0 V	25 µM	5.20 µA mM^{-1} cm^{-2}, 4.56 µA mM^{-1} cm^{-2}	CV and amperometry	Purchased glucose	[173]
Au/SWCNT/rGO/GCE	0.0001–0.030, 0.030–0.6 mM	0.002 µM	N/A	CV and amperometry	Purchased glucose	[174]
Au/FLG/ITO	0.006–28.5 mM @ 1.0 V	1 µM	0.195 µA mM^{-1} cm^{-2}	CV and amperometry	Purchased glucose	[175]
Cu/GTE	0.005–6.0 mM @ 0.55 V	1.6 µM	1100 µA mM^{-1} cm^{-2}	CV	Human serum	[176]
Ni/GNs/GCE	0.005–0.55 mM @ 0.5 V	1.85 µM	865 µA mM^{-1} cm^{-2}	CV and amperometry	N/A	[177]
Cu/rGO/Au platform	0.01–1.2 mM @ 0.55 V	3.4 µM	447.65 µA mM^{-1} cm^{-2}	CV and amperometry	Human serum	[178]
Ni/rGO/GCE	0.001–0.110, 0.001–0.01 mM @ 0.5 V	N/A	813 µA mM^{-1} cm^{-2}, 937 µA mM^{-1} cm^{-2}	CV	N/A	[179]
$Cu(OH)_2$/PGF	0.0012–6 mM @ 0.6 V	1.2 µM	3.36 mA mM^{-1} cm^{-2}	CV and amperometry	Purchased glucose	[180]
Cu_2O/graphene/GCE	0.3–3.3 mM @ 0.6 V	3.3 µM	0.285 mA mM^{-1} cm^{-2}	CV and amperometry	Purchased glucose	[181]
CuO/rGO/GCE	0.0004–12 mM @ 0.4 V	0.1 µM	2221 µA mM^{-1} cm^{-2}	EIS and CV	Purchased glucose	[182]
CuO/rGO/GCE	0.001–6 mM @ 0.55 V	0.50 µM	207.3 µA mM^{-1} cm^{-2}	CV and amperometry	Purchased glucose	[183]
CuO/rGO/CNF/GCE	0.001–5.3 mM @ 0.6 V	0.1 µM	912.7 µA mM^{-1} cm^{-2}	CV and amperometry	N/A	[184]
Cu_2O/rGO/GCE	0.005–2.095, 2.595–9.595 mM @ 0.6 V	1 µM	37.55 µA mM^{-1}, 23.06 µA mM^{-1}	linear sweep voltammetry and amperometry	Purchased glucose	[185]
Cu_2O/rGO/GCE	0.01–0.1 mM @ 0.55 V	N/A	69.5 µA mM^{-1}	CV and amperometry	Purchased glucose	[186]
CuO/graphene/GCE	0.0005–2 mM @ 0.4 V	0.09 µM	2939.24 µA mM^{-1} cm^{-2}	CV and amperometry	Purchased glucose	[187]
Cu_2O/graphene/GCE	0.01–3.0 mM @ 0.5 V	0.36 µM	1330.05 µA mM^{-1} cm^{-2}	CV	Purchased glucose	[188]
CuO/graphene/GCE	0.005–1.4 mM @ 0.5 V	0.2 µM	607 µA mM^{-1} cm^{-2}	CV and amperometry	Purchased glucose	[189]
CuO/graphene/GCE	0.002–4 mM @ 0.55 V	0.7 µM	1360 µA mM^{-1} cm^{-2}	CV and amperometry	Purchased glucose	[190]
CuO/graphene/SPE	0.001–0.5 mM @ 0.6 V	0.034 µM	2367 µA mM^{-1} cm^{-2}	dynamic amperometric	Purchased glucose	[191]
Cu_2O/graphene/GCE	N/A	0.1 µM	N/A	CV and amperometry	N/A	[192]
Co_3O_4/GOH^i/GCE	0.25–10 mM @ 0.62 V	N/A µM	492.8 µA mM^{-1} cm^{-2}	CV and amperometry	real blood	[193]
CO_3O_4/rGOP	0.04–4 mM @ 0.45 V	1.4 µM	1.21 µA mM^{-1} cm^{-2}	CV and amperometry	Purchased glucose	[194]
CO_3O_4/ErGO/GCE	0.01–0.55 mM @ 0.6 V	2 µM	79.3 µA mM^{-1} cm^{-2}	CV and EIS	Purchased glucose	[195]

Table 3. *Cont.*

Electrode Modification	Linear Range	LOD	Sensitivity $mA\ mM^{-1}cm^{-2}$	Principle	Sample	Ref
Ni(II)/Qu/graphene/GCE	0.003–0.9 mM	0.5 µM	187 nA mM^{-1}	CV and amperometry	Purchased glucose	[196]
$Ni(OH)_2$/insulin/rGO/Au platform	0.005–10 mM @ 0.6 V	5 µM	18.9 ± 1.5 mA mM^{-1} cm^{-2}	CV and amperometry	Purchased glucose	[197]
NiO/rGO/GCE	0.002–0.60 mM @ 0.6 V	0.77 µM	1100 µA mM^{-1} cm^{-2}	CV and amperometry	N/A	[198]
NiO/rGO/GCE	0.001–0.4 mM @ 0.6 V	0.18 µM	1138 µA mM^{-1} cm^{-2}	CV and amperometry	Purchased glucose	[199]
$Ni(OH)_2$/rGO/GCE	0.002–3.1 mM @ 0.54 V	0.6 µM	11.43 µA mM^{-1} cm^{-2}	CV and amperometry	Purchased glucose	[200]
$Ni(OH)_2$/graphene/GCE	0.001–0.01, 0.01–0.1 mM @ 0.45 V	0.6 µM	494, 328 µA mM^{-1} cm^{-2}	CV and amperometry	Purchased glucose	[201]
SnO_2/rGO/GCE	0.05–0.5 mM @ 0.8 V	13..35 µM	1.93 A M^{-1} cm^{-2}	CV and amperometry	N/A	[202]
Pt–Au/MnO_2/GP	0.1–30.0 mM @ 0.0 V	20 µM	58.54 µA mM^{-1} cm^{-2}	CV and amperometry	Purchased glucose	[203]
Ni–Co/rGO/GCE	0.01–2.65 mM @ 0.5 V	3.79 µM	1773.61 µA mM^{-1} cm^{-2}	CV and amperometry	Purchased glucose	[204]
Pt–CuO/rGO/SPE	0.005–12 mM @ 0.35 V	0.01 µM	3577 µA mM^{-1} cm^{-2}	LSV and amperometry	Purchased glucose	[205]
NiO/Pt/ErGO/GCE	0.05–5.66 mM @ 0.6 V	0.2 µM	668.2 µA mM^{-1} cm^{-2}	CV and amperometry	Purchased glucose	[206]
Pd–Cu/GRH	1–18 mM @–0.4 V	20 µM	48 µA mg^{-1} cm^{-2}	CV and amperometry	Purchased glucose	[207]
Pt–Ni/graphene/GCE	0.5–20 mM @–0.35 V	2 µM	30.3 µA mM^{-1} cm^{-2}	CV and amperometry	Purchased glucose	[208]
Pt–Pd/IL/rGO/GCE	0.1–22 mM @ 0.0 V	2 µM	1.47 µA mM^{-1} cm^{-2}	CV and amperometry	Purchased glucose	[209]
Pt–Pd/graphene/GCE	0.5–24.5 mM @ 0.2 V	N/A	1.4 µA M^{-1} cm^{-2}	CV and amperometry	Purchased glucose	[210]
Pd/NiO/NB/rGO/CPE	0.02–20 mM @–0.04 V	2.2 µM	N/A	CV and amperometry	Purchased glucose	[211]
Au–CuO/rGO/SPE	0.001–12 mM @ 0.6 V	0.1 µM	2356 µA mM^{-1} cm^{-2}	LSV and amperometry	Purchased glucose	[212]
Pd–CuO/rGO/SPE	0.006–22 mM @ 0.6 V	0.03 µM	3355 µA mM^{-1} cm^{-2}	LSV and amperometry	Purchased glucose	[213]
Pd/Nafion/Graphene/GCE	0.01–5 mM @ 0.4 V	1 µM	N/A	CV and amperometry	Purchased glucose	[214]
Ni/CS/rGO/SPE	0.2–9 mM @ 0.6 V	4.1 µM	318.4 µA mM^{-1} cm^{-2}	CV, chronoamperometry, and EIS	Purchased glucose	[215]
Cu–Co/CS/rGO/GCE	0.015–6.95 mM @ 0.45 V	10 µM	1921 µA mM^{-1} cm^{-2}	CV, chronoamperometry, and amperometry	N/A	[216]
Ni/PEDOT/rGO/GCE	0.001–5.1 mM @ 0.5 V	0.8 µM	36.15 µA mM^{-1} cm^{-2}	EIS, CV, and amperometry	Purchased glucose	[217]
CuO/MnO_2/GO/PVA	0.5–4.4 mM @ 0.4 V	53 µM	N/A	CV	Purchased glucose	[218]
Cu/NG/GCE	0.004–4.5 mM @ 0.5 V	1.3 µM	48.13 µA mM^{-1}	CV and amperometry	Purchased glucose	[219]
Cu–NiO/NG/ITO	0.0002–0.3 mM @ 0.7 V	0.05 µM	7.49 µA mM^{-1} cm^{-2}	CV, amperometry, and EIS	Purchased glucose	[220]
Mn_3O_4/NG/CPE	0.0025–0.5295 mM @ 0.9 V	1.0 µM	0.1011 µA $µM^{-1}$	CV, amperometry, and EIS	Purchased glucose	[221]
Mn_3O_4/N-rGO/GCE	0.001–0.3295 mM @ 0.7 V	0.5 µM	0.026 µA $µM^{-1}$	CV, amperometry, and EIS	N/A	[222]
CuO/SG	0.1–10.5 mM @ 0.5 V	0.08 µM	1298.6 µA mM^{-1}	CV, amperometry, and EIS	Purchased glucose	[95]

Thi: Thionine; GO: Graphene oxide; GCE: Glassy carbon electrode; BSA: Bovine serum albumin; rGO: Reduced graphene oxide; IL: Ionic liquid; SCCO2: Supercritical CO2 fluid; GONR: Graphene oxide nanoribbon; CS: Carbon sheet substrate; GA: Graphene aerogel; GOH: Graphene oxide hydrogel; SWCNT: Single-walled carbon nanotubes; FLG: Few-layered graphene; ITO: Indium tin oxide; GTE: Graphene transparent electrode; GNs: Graphene nanosheet; ATP: Attapulgite; DLEG: Direct laser engraved graphene; PGF: Porous graphene foam; CNF: Carbon nanofiber; SPE: Screen printed electrode; rGOP: Reduced graphene oxide paste; ErGO: Electrochemically reduced graphene oxide; Qu: Quercetin; GP: Graphene paper; NB: Nile blue; CPE: Carbon paste electrode; PrGO: Porous reduced graphene oxide; CS: Chitosan; PEDOT: Poly(3,4-ethylenedioxythiophene); PVA: Polyvinyl alcohol; NG: Nitrogen-doped graphene; ITO: Indium doped tin oxide; CPE: Carbon paste electrode; N-rGO: Nitrogen-doped reduced graphene oxide; SG: Sulfur-doped graphene.

6. Conclusions

The CV detection technique is a way for electrochemical characterization of the electrode's performance towards a very specific molecule. The non-enzymatic glucose sensor normally uses this technology for analysis purposes of the glucose. Graphene-based nanocomposites are widely used in non-enzymatic glucose sensors because of their unique properties, sensitivity, cost-effective, and green purpose. Despite the scientific effort, the graphene-based electrode for the portable non-enzymatic glucose sensor has not been developed yet. While a few numbers of articles in this field focus on the preparation of new electrodes based on graphene that could be applicable for electrochemical reactions, the understanding limitation of the material reaction with the glucose directly affects the large-scale production. The understanding of the reaction between the graphene nanocomposites and glucose would give a chance to develop rapidly. To do so, the ISO standard should be followed. There are basic components that need to be tested during the experiments; selectivity (must select the target only), sensitivity for the target, no oxygen-dependent, stability, accuracy, precision, low cost, biocompatibility, and easy fabrication. However, graphene and its nanocomposites still promise many chances for future non-enzymatic glucose sensor development. The unique electrochemical properties of graphene-based non-enzymatic glucose sensors make the scalability the first concern for a high scale production with successful commercialization. Despite many ways that have been demonstrated for graphene fabrication, there are not enough methods that could produce graphene at a low-cost demand. Hence, the CVD method is promising for cost-effectiveness, high scale production, which could be used directly for the fabrication of non-enzymatic glucose sensor systems at low cost. The electrocatalytic activities of the graphene-based non-enzymatic glucose sensor depend on the graphene structure (purity), still, there is a lack of information and understanding for these details, which means there are many things that should be detailed for this issue. Although the low experimental efforts were investigated for low-contact resistance between the catalyst and current collector, the high resistance was still maintained as a barrier for the highly efficient non-enzymatic glucose sensors. The limitation of the study for most research efforts on graphene sheets makes the possibility of rapid progress low. There is a huge chance of making high-performance non-enzymatic glucose sensors if the research is considered for nanoparticles, dots, ribbons, etc. The rapid progress in graphene-based non-enzymatic glucose sensors will lead to the fourth generation of sensors that could be implemented for bio-information sensors and microfluidic chips. Somehow, this could help the patient.

Author Contributions: W.C., formal analysis, writing—review and editing, visualization, supervision, and funding acquisition; M.H.F.T., the formal author, conceptualization, formal investigation, writing—review and editing, and project administration; H.A., a second author, formal writing and editing. All authors have read and agreed to the published version of the manuscript.

Funding: This research received no external funding.

Acknowledgments: The author has submitted some parts of this work as a part of the Postgraduate Certificate of Nanotechnology at the department of continuing education, the University of Oxford, UK. The work was titled "Cyclic voltammetry transducer for biosensors." The Article Processing Charge (APC) of this paper is funded by Wahyu Caesarendra.

Conflicts of Interest: The authors declare no conflict of interest.

References

1. Patolsky, F.; Zheng, G.; Lieber, C.M. Nanowire sensors for medicine and the life sciences. *Nanomedicine* **2006**, *1*, 51–65. [CrossRef] [PubMed]
2. Peña-Bahamonde, J.; Nguyen, H.N.; Fanourakis, S.K.; Rodrigues, D.F. Recent advances in graphene-based biosensor technology with applications in life sciences. *J. Nanobiotechnol.* **2018**, *16*, 75. [CrossRef] [PubMed]
3. Sapsford, K.E.; Bradburne, C.; Delehanty, J.B.; Medintz, I.L. Sensors for detecting biological agents. *Mater. Today* **2008**, *11*, 38–49. [CrossRef]
4. Wilson, C.B. Sensors in medicine. *BMJ* **1999**, *319*, 1288. [CrossRef] [PubMed]

5. Zhu, Y.; Murali, S.; Cai, W.; Li, X.; Suk, J.W.; Potts, J.R.; Ruoff, R.S. Graphene and Graphene Oxide: Synthesis, Properties, and Applications. *Adv. Mater.* **2010**, *22*, 3906–3924. [CrossRef]
6. Malik, P.; Katyal, V.; Malik, V.; Asatkar, A.; Inwati, G.; Mukherjee, T.K. Nanobiosensors: Concepts and Variations. *ISRN Nanomater.* **2013**, *2013*, 1–9. [CrossRef]
7. Touhami, A. Biosensors and Nanobiosensors: Design and Applications. *Nanomedicine* **2014**, *15*, 374–403.
8. Ahlatcioglu Özerol, E.A.Ö.; İpek, Y. *Biosensors and Their Principles, A Roadmap of Biomedical Engineers and Milestones*; InTech: Vienna, Austria, 2012; Available online: https://www.researchgate.net/publication/280614632_Biosensors_and_Their_Principles (accessed on 30 July 2020).
9. Grutter, P. An Introduction to Micromachined Biochemical Sensors-PPT Download. 2015. Available online: https://slideplayer.com/slide/6368321/ (accessed on 31 July 2020).
10. Nikhil, B.; Pawan, J.; Nello, F.; Pedro, E. Introduction to Biosensor. *Essays Biochem.* **2016**, *60*, 1–8.
11. Lin, H.-Y.; Chen, W.-H.; Huang, C.-H. *Graphene in Electrochemical Biosensors. Biomedical Applications of Graphene and 2D Nanomaterials*; Elsevier: Amsterdam, The Netherlands, 2019; pp. 321–336.
12. Wang, C.-F.; Sun, X.-Y.; Su, M.; Wang, Y.-P.; Lv, Y.-K. Electrochemical biosensors based on antibody, nucleic acid and enzyme functionalized graphene for the detection of disease-related biomolecules. *Analyst* **2020**, *145*, 1550–1562. [CrossRef]
13. Yang, C.; Denno, M.E.; Pyakurel, P.; Venton, B.J. Recent trends in carbon nanomaterial-based electrochemical sensors for biomolecules: A review. *Anal. Chim. Acta* **2015**, *887*, 17–37. [CrossRef]
14. Justino, C.I.; Gomes, A.R.; Freitas, A.C.; Duarte, A.C.; Rocha-Santos, T. Graphene based sensors and biosensors. *TrAC Trends Anal. Chem.* **2017**, *91*, 53–66. [CrossRef]
15. Pirzada, M.; Altintas, Z. Nanomaterials for Healthcare Biosensing Applications. *Sensors* **2019**, *19*, 5311. [CrossRef] [PubMed]
16. Mansuriya, B.D.; Altintas, Z. Graphene Quantum Dot-Based Electrochemical Immunosensors for Biomedical Applications. *Materials* **2019**, *13*, 96. [CrossRef] [PubMed]
17. Zhu, H.; Li, L.; Zhou, W.; Shao, Z.; Chen, X. Advances in non-enzymatic glucose sensors based on metal oxides. *J. Mater. Chem. B* **2016**, *4*, 7333–7349. [CrossRef] [PubMed]
18. Kumar, H.; Kuca, K.; Bhatia, S.K.; Saini, K.; Kaushal, A.; Verma, R.; Bhalla, T.C.; Kumar, D. Applications of Nanotechnology in Sensor-Based Detection of Foodborne Pathogens. *Sensors* **2020**, *20*, 1966. [CrossRef]
19. Clark, L.C.; Lyons, C. ELECTRODE SYSTEMS FOR CONTINUOUS MONITORING IN CARDIOVASCULAR SURGERY. *Ann. N. Y. Acad. Sci.* **2006**, *102*, 29–45. [CrossRef]
20. Hale, P.D.; Inagaki, T.; Karan, H.I.; Okamoto, Y.; Skotheim, T.A. A new class of amperometric biosensor incorporating a polymeric electron-transfer mediator. *J. Am. Chem. Soc.* **1989**, *111*, 3482–3484. [CrossRef]
21. Cass, A.E.G.; Davis, G.; Francis, G.D.; Hill, H.A.O.; Aston, W.J.; Higgins, I.J.; Plotkin, E.V.; Scott, L.D.L.; Turner, A.P. Ferrocene-mediated enzyme electrode for amperometric determination of glucose. *Anal. Chem.* **1984**, *56*, 667–671. [CrossRef]
22. Wang, J. Electrochemical Glucose Biosensors. *Chem. Rev.* **2008**, *108*, 814–825. [CrossRef]
23. Liu, J.; Guo, C.X.; Li, C.M.; Li, Y.; Chi, Q.; Huang, X.; Liao, L.; Yu, T. Carbon-decorated ZnO nanowire array: A novel platform for direct electrochemistry of enzymes and biosensing applications. *Electrochem. Commun.* **2009**, *11*, 202–205. [CrossRef]
24. Xiao, Y.; Patolsky, F.; Katz, E.; Hainfeld, J.F.; Willner, I. "Plugging into Enzymes": Nanowiring of Redox Enzymes by a Gold Nanoparticle. *Science* **2003**, *299*, 1877–1881. [CrossRef]
25. Wilson, R.; Turner, A.P. Glucose oxidase: An ideal enzyme. *Biosens. Bioelectron.* **1992**, *7*, 165–185. [CrossRef]
26. Li, J.; Lin, X. Glucose biosensor based on immobilization of glucose oxidase in poly(o-aminophenol) film on polypyrrole-Pt nanocomposite modified glassy carbon electrode. *Biosens. Bioelectron.* **2007**, *22*, 2898–2905. [CrossRef] [PubMed]
27. Wu, B.; Zhang, G.; Shuang, S.; Choi, M.M.F. Biosensors for determination of glucose with glucose oxidase immobilized on an eggshell membrane. *Talanta* **2004**, *64*, 546–553. [CrossRef]
28. Han, K.; Wu, Z.; Lee, J.; Ahn, I.-S.; Park, J.W.; Min, B.R.; Lee, K. Activity of glucose oxidase entrapped in mesoporous gels. *Biochem. Eng. J.* **2005**, *22*, 161–166. [CrossRef]
29. Ohara, T.J.; Rajagopalan, R.; Heller, A. "Wired" Enzyme Electrodes for Amperometric Determination of Glucose or Lactate in the Presence of Interfering Substances. *Anal. Chem.* **1994**, *66*, 2451–2457. [CrossRef] [PubMed]

30. Hammond, J.L.; Formisano, N.; Carrara, S.; Tkac, J. Electrochemical biosensors and nanobiosensors. *Essays Biochem.* **2016**, *60*, 69–80. [CrossRef] [PubMed]
31. Toghill, K.E.; Compton, R.G. Electrochemical Non-enzymatic Glucose Sensors: A Perspective and an Evaluation. 2010. Available online: https://www.semanticscholar.org/paper/Electrochemical-non-enzymatic-glucose-sensors%3Aa-and-Toghill-Compton/23e793fd60eca87ddf9f0e63587d3368ff5c6eed (accessed on 31 July 2020).
32. Park, S.; Boo, H.; Chung, T.D. Electrochemical non-enzymatic glucose sensors. *Anal. Chim. Acta* **2006**, *556*, 46–57. [CrossRef]
33. Chen, X.; Wu, G.; Cai, Z.; Oyama, M.; Chen, X. Advances in enzyme-free electrochemical sensors for hydrogen peroxide, glucose, and uric acid. *Microchim. Acta* **2013**, *181*, 689–705. [CrossRef]
34. Carbone, M.; Gorton, L.; Antiochia, R. An Overview of the Latest Graphene-Based Sensors for Glucose Detection: The Effects of Graphene Defects. *Electroanalysis* **2015**, *27*, 16–31. [CrossRef]
35. Favero, G.; Fusco, G.; Mazzei, F.; Tasca, F.; Antiochia, R. Electrochemical Characterization of Graphene and MWCNT Screen-Printed Electrodes Modified with AuNPs for Laccase Biosensor Development. *Nanomaterials* **2015**, *5*, 1995–2006. [CrossRef] [PubMed]
36. Gao, H.; Duan, H. 2D and 3D graphene materials: Preparation and bioelectrochemical applications. *Biosens. Bioelectron.* **2015**, *65*, 404–419. [CrossRef] [PubMed]
37. Song, Y.; Luo, Y.; Zhu, C.; Li, H.; Dub, D.; Linb, Y. Recent advances in electrochemical biosensors based on graphene two-dimensional nanomaterials. *Biosens. Bioelectron.* **2016**, *76*, 195–212. [CrossRef] [PubMed]
38. Geim, A.K.; Novoselov, K.S. The rise of graphene. *Nat. Mater.* **2007**, *6*, 183–191. [CrossRef] [PubMed]
39. Mao, H.Y.; Laurent, S.; Chen, W.; Akhavan, O.; Imani, M.; Ashkarran, A.A.; Mahmoudi, M. Graphene: Promises, Facts, Opportunities, and Challenges in Nanomedicine. *Chem. Rev.* **2013**, *113*, 3407–3424. [CrossRef]
40. Sehrawat, P.; Islam, S.S.; Mishra, P.; Ahmad, S. Abid Reduced graphene oxide (rGO) based wideband optical sensor and the role of Temperature, Defect States and Quantum Efficiency. *Sci. Rep.* **2018**, *8*, 1–13. [CrossRef]
41. Pumera, M.; Ambrosi, A.; Bonanni, A.; Chng, E.L.K.; Poh, H.L. Graphene for electrochemical sensing and biosensing. *TrAC Trends Anal. Chem.* **2010**, *29*, 954–965. [CrossRef]
42. Thévenot, D.R.; Toth, K.; Durst, R.A.; Wilson, G.S. Electrochemical Biosensors: Recommended Definitions and Classification1International Union of Pure and Applied Chemistry: Physical Chemistry Division, Commission I.7 (Biophysical Chemistry); Analytical Chemistry Division, Commission V.5 (Electroanalytical Chemistry).1. *Biosens. Bioelectron.* **2001**, *16*, 121–131.
43. Grieshaber, D.; MacKenzie, R.; Vörös, J.; Reimhult, E. Electrochemical Biosensors - Sensor Principles and Architectures. *Sensors* **2008**, *8*, 1400–1458. [CrossRef]
44. Stankovich, S.; Dikin, D.A.; Piner, R.D.; Kohlhaas, K.A.; Kleinhammes, A.; Jia, Y.; Wu, Y.; Nguyen, S.T.; Ruoff, R.S. Synthesis of graphene-based nanosheets via chemical reduction of exfoliated graphite oxide. *Carbon* **2007**, *45*, 1558–1565. [CrossRef]
45. Wilson, N.R.; Pandey, P.A.; Beanland, R.; Young, R.J.; Kinloch, I.A.; Gong, L.; Liu, Z.; Suenaga, K.; Rourke, J.P.; York, S.J.; et al. Graphene Oxide: Structural Analysis and Application as a Highly Transparent Support for Electron Microscopy. *ACS Nano* **2009**, *3*, 2547–2556. [CrossRef]
46. Bagri, A.; Mattevi, C.; Acik, M.; Chabal, Y.J.; Chhowalla, M.; Shenoy, V.B. Structural evolution during the reduction of chemically derived graphene oxide. *Nat. Chem.* **2010**, *2*, 581–587. [CrossRef] [PubMed]
47. Paredes, J.; Villar-Rodil, S.; Martinez-Alonso, A.; Tascón, J.D. Graphene Oxide Dispersions in Organic Solvents. *Langmuir* **2008**, *24*, 10560–10564. [CrossRef] [PubMed]
48. Lightcap, I.; Kosel, T.H.; Kamat, P.V. Anchoring Semiconductor and Metal Nanoparticles on a Two-Dimensional Catalyst Mat. Storing and Shuttling Electrons with Reduced Graphene Oxide. *Nano Lett.* **2010**, *10*, 577–583. [CrossRef] [PubMed]
49. Yang, D.; Velamakanni, A.; Bozoklu, G.; Park, S.; Stoller, M.; Piner, R.D.; Stankovich, S.; Jung, I.; Field, D.A.; Ventrice, C.A.; et al. Chemical analysis of graphene oxide films after heat and chemical treatments by X-ray photoelectron and Micro-Raman spectroscopy. *Carbon* **2009**, *47*, 145–152. [CrossRef]
50. Khan, Q.A.; Shaur, A.; Khan, T.A.; Joya, Y.F.; Awan, M. Characterization of reduced graphene oxide produced through a modified Hoffman method. *Cogent Chem.* **2017**, *3*, 1298980. [CrossRef]
51. Gilje, S.; Han, S.; Wang, M.; Wang, K.L.; Kaner, R.B. A Chemical Route to Graphene for Device Applications. *Nano Lett.* **2007**, *7*, 3394–3398. [CrossRef]

52. Montes-Navajas, P.; Asenjo, N.G.; Santamaria, R.; Menendez, R.; Corma, A.; Garcia, H. Surface Area Measurement of Graphene Oxide in Aqueous Solutions. *Langmuir* **2013**, *29*, 13443–13448. [CrossRef]
53. Khan, M.; Tahir, M.N.; Adil, S.F.; Khan, H.U.; Siddiqui, M.R.; Kuniyil, M.; Tremel, W. Graphene based metal and metal oxide nanocomposites: Synthesis, properties and their applications. *J. Mater. Chem. A* **2015**, *3*, 18753–18808. [CrossRef]
54. Singh, V.; Joung, D.; Zhai, L.; Das, S.; Khondaker, S.I.; Seal, S. Graphene based materials: Past, present and future. *Prog. Mater. Sci.* **2011**, *56*, 1178–1271. [CrossRef]
55. Renteria, J.D.; Ramirez, S.; Malekpour, H.; Alonso, B.; Centeno, A.; Zurutuza, A.; I Cocemasov, A.; Nika, D.L.; Balandin, A.A. Strongly Anisotropic Thermal Conductivity of Free-Standing Reduced Graphene Oxide Films Annealed at High Temperature. *Adv. Funct. Mater.* **2015**, *25*, 4664–4672. [CrossRef]
56. Mahanta, N.K.; Abramson, A.R. Thermal conductivity of graphene and graphene oxide nanoplatelets. In *Proceedings of the 13th InterSociety Conference on Thermal and Thermomechanical Phenomena in Electronic Systems, San Diego, CA, USA, 30 May–1 June 2012*; Institute of Electrical and Electronics Engineers (IEEE): Piscataway, NJ, USA, 2012; pp. 1–6.
57. Kumar, P.; Shahzad, F.; Yu, S.; Hong, S.M.; Kim, Y.-H.; Koo, C.M. Large-area reduced graphene oxide thin film with excellent thermal conductivity and electromagnetic interference shielding effectiveness. *Carbon* **2015**, *94*, 494–500. [CrossRef]
58. Kumar, S.; Kumar, S.; Srivastava, S.; Yadav, B.K.; Lee, S.H.; Sharma, J.G.; Doval, D.C.; Malhotra, B. Reduced graphene oxide modified smart conducting paper for cancer biosensor. *Biosens. Bioelectron.* **2015**, *73*, 114–122. [CrossRef]
59. Neto, A.H.C.; Guinea, F.; Peres, N.M.R.; Novoselov, K.S.; Geim, A.K. The electronic properties of graphene. *Rev. Mod. Phys.* **2009**, *81*, 109–162. [CrossRef]
60. Zhao, Y.; Liu, J.; Wang, B.; Sha, J.; Li, Y.; Zheng, D.; Amjadipour, M.; MacLeod, J.; Motta, N. Supercapacitor Electrodes with Remarkable Specific Capacitance Converted from Hybrid Graphene Oxide/NaCl/Urea Films. *ACS Appl. Mater. Interfaces* **2017**, *9*, 22588–22596. [CrossRef]
61. Ojha, K.; Kumar, B.; Ganguli, A. Biomass derived graphene-like activated and non-activated porous carbon for advanced supercapacitors. *J. Chem. Sci.* **2017**, *129*, 397–404. [CrossRef]
62. Chen, Y.; Zhang, X.; Zhang, D.; Yu, P.; Ma, Y.-W. High performance supercapacitors based on reduced graphene oxide in aqueous and ionic liquid electrolytes. *Carbon* **2011**, *49*, 573–580. [CrossRef]
63. Ke, Q.; Liu, Y.; Liu, H.; Zhang, Y.; Hu, Y.; Wang, J. Surfactant-modified chemically reduced graphene oxide for electrochemical supercapacitors. *RSC Adv.* **2014**, *4*, 26398–26406. [CrossRef]
64. Yun, Y.S.; Yoon, G.; Park, M.; Cho, S.Y.; Lim, H.-D.; Kim, H.; Park, Y.W.; Kim, B.H.; Kang, K.; Jin, H.-J. Restoration of thermally reduced graphene oxide by atomic-level selenium doping. *NPG Asia Mater.* **2016**, *8*, e338. [CrossRef]
65. Benchirouf, A.; Müller, C.; Kanoun, O. Electromechanical Behavior of Chemically Reduced Graphene Oxide and Multi-walled Carbon Nanotube Hybrid Material. *Nanoscale Res. Lett.* **2016**, *11*, 1–7. [CrossRef]
66. Chen, W.; Yan, L.; Bangal, P.R. Chemical Reduction of Graphene Oxide to Graphene by Sulfur-Containing Compounds. *J. Phys. Chem. C* **2010**, *114*, 19885–19890. [CrossRef]
67. Goumri, M.; Lucas, B.; Ratier, B.; Baitoul, M. Electrical and optical properties of reduced graphene oxide and multi-walled carbon nanotubes based nanocomposites: A comparative study. *Opt. Mater.* **2016**, *60*, 105–113. [CrossRef]
68. De, S.; Coleman, J.N. Are There Fundamental Limitations on the Sheet Resistance and Transmittance of Thin Graphene Films? *ACS Nano* **2010**, *4*, 2713–2720. [CrossRef] [PubMed]
69. Liuab, J.; Tang, J.; Gooding, J.J. Strategies for chemical modification of graphene and applications of chemically modified graphene. *J. Mater. Chem.* **2012**, *22*, 12435. [CrossRef]
70. Morales-Narváez, E.; Baptista-Pires, L.; Zamora-Gálvez, A.; Merkoçi, A. Graphene-Based Biosensors: Going Simple. *Adv. Mater.* **2016**, *29*, 1604905. [CrossRef]
71. Chauhan, N.; Maekawa, T.; Sakthikumar, D.N. Graphene based biosensors—Accelerating medical diagnostics to new-dimensions. *J. Mater. Res.* **2017**, *32*, 2860–2882. [CrossRef]
72. Janegitz, B.C.; Silva, T.A.; Wong, A.; Ribovski, L.; Vicentini, F.C.; Sotomayor, M.D.P.; Fatibello-Filho, O. The application of graphene for in vitro and in vivo electrochemical biosensing. *Biosens. Bioelectron.* **2017**, *89*, 224–233. [CrossRef]

73. Wang, Y.; Li, Z.; Wang, J.; Li, J.; Lin, Y. Graphene and graphene oxide: Biofunctionalization and applications in biotechnology. *Trends Biotechnol.* **2011**, *29*, 205–212. [CrossRef]
74. Pumera, M. Graphene in biosensing. *Mater. Today.* **2011**, *14*, 308–315. [CrossRef]
75. Sabine, S.; Boukherroub, R. Graphene-Based Biosensors. *Interface Focus* **2018**, *8*, 20160132. [CrossRef]
76. Park, C.S.; Yoon, H.; Kwon, O. Graphene-based nanoelectronic biosensors. *J. Ind. Eng. Chem.* **2016**, *38*, 13–22. [CrossRef]
77. Kuila, T.; Bose, S.; Khanra, P.; Mishra, A.K.; Kim, N.H.; Lee, J.H. Recent advances in graphene-based biosensors. *Biosens. Bioelectron.* **2011**, *26*, 4637–4648. [CrossRef]
78. Rao, C.N.R.; Sood, A.K.; Subrahmanyam, K.S.; Govindaraj, A. Graphene: The New Two-Dimensional Nanomaterial. *Angew. Chem. Int. Ed.* **2009**, *48*, 7752–7777. [CrossRef] [PubMed]
79. Lawal, A.T. Progress in utilisation of graphene for electrochemical biosensors. *Biosens. Bioelectron.* **2018**, *106*, 149–178. [CrossRef] [PubMed]
80. Thévenot, D.R.; Toth, K.; Durst, R.A.; Wilson, G.S. Electrochemical biosensors: Recommended definitions and classification. *Biosens. Bioelectron.* **2001**, *16*, 121–131. [CrossRef]
81. Rao, H.; Zhang, Z.; Ge, H.; Liu, X.; Zou, P.; Wang, X.; Wang, Y. Enhanced amperometric sensing using a NiCo2O4/nitrogen-doped reduced graphene oxide/ionic liquid ternary composite for enzyme-free detection of glucose. *New J. Chem.* **2017**, *41*, 3667–3676. [CrossRef]
82. Zhang, X.; Ju, H.; Wang, J. *Electrochemical Sensors, Biosensors and their Biomedical Applications*; Elsevier: Amsterdam, The Netherlands, 2008.
83. Chemistry. Cyclic Voltammetry. Chemistry LibreTexts. 2013. Available online: https://chem.libretexts.org/Bookshelves/Analytical_Chemistry/Supplemental_Modules(Analytical_Chemistry)/Instrumental_Analysis/Cyclic_Voltammetry (accessed on 30 June 2020).
84. Chooto, P. Cyclic Voltammetry and Its Applications. Voltammetry. 2019. Available online: https://www.intechopen.com/books/voltammetry/cyclic-voltammetry-and-its-applications (accessed on 30 June 2020).
85. Lee, K.J.; Elgrishi, N.; Kandemir, B.; Dempsey, J.L. Electrochemical and spectroscopic methods for evaluating molecular electrocatalysts. *Nat. Rev. Chem.* **2017**, *1*, 39. [CrossRef]
86. Anonymous. Introduction. 2019. Available online: https://www.ceb.cam.ac.uk/research/groups/rg-eme/Edu/introduction (accessed on 30 June 2020).
87. Sudhakar, Y.N.; Selvakumar, M.; Bhat, D.K. *Biopolymer Electrolytes: Fundamentals and Applications in Energy Storage*; Elsevier: Amsterdam, The Netherlands, 2018.
88. Elgrishi, N.; Rountree, K.J.; McCarthy, B.D.; Rountree, E.; Eisenhart, T.T.; Dempsey, J.L. A Practical Beginner's Guide to Cyclic Voltammetry. *J. Chem. Educ.* **2017**, *95*, 197–206. [CrossRef]
89. Brain, R. Chemical Sensors and Biosensors. Google Books. 2020. Available online: https://books.google.com.eg/books?hl=en&lr=&id=54PcKt5bT58C&oi=fnd&pg=PP1&ots=ZtZ1AAQXIV&sig=Cv449j0WGXnn8tDNatVjLZYFuV0&redir_esc=y#v=onepage&q&f=false (accessed on 30 June 2020).
90. Heyrovský, J. The development of polarographic analysis. *Analyst* **1956**, *81*, 189–192. [CrossRef]
91. Pei, R.; Cheng, Z.; Wang, E.; Yang, X. Amplification of antigen–antibody interactions based on biotin labeled protein–streptavidin network complex using impedance spectroscopy. *Biosens. Bioelectron.* **2001**, *16*, 355–361. [CrossRef]
92. Li, Y.; Tremblay, P.-L.; Zhang, T. Anode Catalysts and Biocatalysts for Microbial Fuel Cells. In *Progress and Recent Trends in Microbial Fuel Cells*; Elsevier: Amsterdam, The Netherlands, 2018; pp. 143–165. Available online: https://www.sciencedirect.com/science/article/pii/B9780444640178000099 (accessed on 30 June 2020).
93. PS, J.; Sutrave, D.S. A Brief Study of Cyclic Voltammetry and Electrochemical Analysis. *Int. J. ChemTech Res.* **2018**, *11*, 77–88. [CrossRef]
94. Veloso, A.J.; Cheng, X.R.; Kerman, K. Electrochemical biosensors for medical applications. In *Biosensors for Medical Applications*; Woodhead Publishing: Sawston, UK, 2012; Available online: www.sciencedirect.com/science/article/pii/B9781845699352500012 (accessed on 30 June 2020).
95. Tian, Y.; Liu, Y.; Wang, W.-P.; Zhang, X.; Peng, W. CuO nanoparticles on sulfur-doped graphene for nonenzymatic glucose sensing. *Electrochim. Acta* **2015**, *156*, 244–251. [CrossRef]
96. Luan, V.H.; Han, J.H.; Kang, H.W.; Lee, W. Ultra-sensitive non-enzymatic amperometric glucose sensors based on silver nanowire/graphene hybrid three-dimensional nanostructures. *Results Phys.* **2019**, *15*, 102761. [CrossRef]

97. Sreejesh, M.; Dhanush, S.; Rossignol, F.; Nagaraja, H. Microwave assisted synthesis of rGO/ZnO composites for non-enzymatic glucose sensing and supercapacitor applications. *Ceram. Int.* **2017**, *43*, 4895–4903. [CrossRef]
98. Taniselass, S.; Arshad, M.M.; Gopinath, S.C. Graphene-based electrochemical biosensors for monitoring noncommunicable disease biomarkers. *Biosens. Bioelectron.* **2019**, *130*, 276–292. [CrossRef]
99. Lee, J.-H.; Park, S.-J.; Choi, J.-W. Electrical Property of Graphene and Its Application to Electrochemical Biosensing. *Nanomater.* **2019**, *9*, 297. [CrossRef]
100. Xu, J.; Wang, Y.; Hu, S. Nanocomposites of graphene and graphene oxides: Synthesis, molecular functionalization and application in electrochemical sensors and biosensors. A review. *Microchim. Acta* **2016**, *184*, 1–44. [CrossRef]
101. Wang, X.-Y.; Narita, A.; Müllen, K. Precision synthesis versus bulk-scale fabrication of graphenes. *Nat. Rev. Chem.* **2017**, *2*, 100. [CrossRef]
102. Bonanni, A.; Loo, A.H.; Pumera, M. Graphene for impedimetric biosensing. *TrAC Trends Anal. Chem.* **2012**, *37*, 12–21. [CrossRef]
103. Wei, D.; Liu, Y. Controllable Synthesis of Graphene and Its Applications. *Adv. Mater.* **2010**, *22*, 3225–3241. [CrossRef]
104. Xu, C.; Shi, X.; Ji, A.; Shi, L.; Zhou, C.; Cui, Y. Fabrication and Characteristics of Reduced Graphene Oxide Produced with Different Green Reductants. *PLoS ONE* **2015**, *10*, e0144842. [CrossRef] [PubMed]
105. Yang, J.; Deng, S.; Lei, J.; Ju, H.; Gunasekaran, S. Electrochemical synthesis of reduced graphene sheet–AuPd alloy nanoparticle composites for enzymatic biosensing. *Biosens. Bioelectron.* **2011**, *29*, 159–166. [CrossRef] [PubMed]
106. Tan, L.-L.; Ong, W.-J.; Chai, S.-P.; Mohamed, A.R. Photocatalytic reduction of CO 2 with H 2 O over graphene oxide-supported oxygen-rich TiO 2 hybrid photocatalyst under visible light irradiation: Process and kinetic studies. *Chem. Eng. J.* **2017**, *308*, 248–255. [CrossRef]
107. Voiry, D.; Yang, J.; Kupferberg, J.; Fullon, R.; Lee, C.; Jeong, H.Y.; Shin, H.S.; Chhowalla, M. High-quality graphene via microwave reduction of solution-exfoliated graphene oxide. *Science* **2016**, *353*, 1413–1416. [CrossRef]
108. Faucett, A.C.; Flournoy, J.N.; Mehta, J.S.; Mativetsky, J.M. Evolution, structure, and electrical performance of voltage-reduced graphene oxide. *FlatChem* **2017**, *1*, 42–51. [CrossRef]
109. Luo, D.; Zhang, G.; Liu, J.; Sun, X. Evaluation Criteria for Reduced Graphene Oxide. *J. Phys. Chem. C* **2011**, *115*, 11327–11335. [CrossRef]
110. Akolpoglu, M.B.; Bozuyuk, U.; Erkoc, P.; Kizilel, S. Biosensing–Drug Delivery Systems for In Vivo Applications. In *Advanced Biosensors for Health Care Applications*; Elsevier: Amsterdam, The Netherlands, 2019; Available online: www.sciencedirect.com/science/article/pii/B9780128157435000093 (accessed on 29 July 2020).
111. Lawal, A.T. Synthesis and utilisation of graphene for fabrication of electrochemical sensors. *Talanta* **2015**, *131*, 424–443. [CrossRef]
112. Thangamuthu, M.; Hsieh, K.Y.; Kumar, P.V.; Chen, G.-Y. Graphene- and Graphene Oxide-Based Nanocomposite Platforms for Electrochemical Biosensing Applications. *Int. J. Mol. Sci.* **2019**, *20*, 2975. [CrossRef]
113. Ciesielski, A.; Samorì, P. Grapheneviasonication assisted liquid-phase exfoliation. *Chem. Soc. Rev.* **2014**, *43*, 381–398. [CrossRef]
114. Gomez, C.V.; Tene, T.; Guevara, M.; Usca, G.T.; Colcha, D.; Brito, H.; Molina, R.; Bellucci, S.; Tavolaro, A. Preparation of Few-Layer Graphene Dispersions from Hydrothermally Expanded Graphite. *Appl. Sci.* **2019**, *9*, 2539. [CrossRef]
115. Ou, E.-C.; Xie, Y.; Peng, C.; Peng, H.; Xiong, Y.; Song, Y.; Xu, W. High concentration and stable few-layer graphene dispersions prepared by the exfoliation of graphite in different organic solvents. *RSC Adv.* **2013**, *3*, 9490. [CrossRef]
116. Liu, F.; Wang, C.; Sui, X.; Riaz, M.A.; Xu, M.; Wei, L.; Chen, Y. Synthesis of graphene materials by electrochemical exfoliation: Recent progress and future potential. *Carbon Energy* **2019**, *1*, 173–199. [CrossRef]
117. Resmi, P.; Palaniayappan, A.; Ramachandran, T.; Babu, T.S. Electrochemical synthesis of graphene and its application in electrochemical sensing of glucose. *Mater. Today Proc.* **2018**, *5*, 16487–16493. [CrossRef]

118. Balasubramanian, P.; Velmurugan, M.; Chen, S.-M.; Hwa, K.-Y. Optimized electrochemical synthesis of copper nanoparticles decorated reduced graphene oxide: Application for enzymeless determination of glucose in human blood. *J. Electroanal. Chem.* **2017**, *807*, 128–136. [CrossRef]
119. Shao, Y.; Wang, J.; Wu, H.; Liu, J.; Aksay, I.A.; Lin, Y. Graphene based electrochemical sensors and biosensors: A review. *Electroanal. Int. J. Devoted Fundam. Pract. Asp. Electroanal.* **2010**, *22*, 1027–1036. [CrossRef]
120. Marcano, D.C.; Kosynkin, D.V.; Berlin, J.M.; Sinitskii, A.; Sun, Z.; Slesarev, A.; Alemany, L.B.; Lu, W.; Tour, J.M. Improved synthesis of graphene oxide. *ACS Nano* **2010**, *4*, 4806–4814. [CrossRef] [PubMed]
121. De Heer, W.A.; Berger, C.; Ruan, M.; Sprinkle, M.; Li, X.; Hu, Y.; Zhang, B.; Hankinson, J.; Conrad, E. Large area and structured epitaxial graphene produced by confinement controlled sublimation of silicon carbide. *Proc. Natl. Acad. Sci. USA* **2011**, *108*, 16900–16905. [CrossRef] [PubMed]
122. Kang, J.; Shin, D.; Bae, S.; Hong, B.H. Graphene transfer: Key for applications. *Nanoscale* **2012**, *4*, 5527. [CrossRef]
123. Chen, T.-Y.; Loan, P.T.K.; Hsu, C.-L.; Lee, Y.-H.; Wang, J.T.-W.; Wei, K.H.; Lin, C.-T.; Li, L.-J. Label-free detection of DNA hybridization using transistors based on CVD grown graphene. *Biosens. Bioelectron.* **2013**, *41*, 103–109. [CrossRef]
124. Wu, W.; Liu, Z.; Jauregui, L.A.; Yu, Q.; Pillai, R.; Cao, H.; Bao, J.; Chen, Y.P.; Pei, S.-S. Wafer-scale synthesis of graphene by chemical vapor deposition and its application in hydrogen sensing. *Sens. Actuators B Chem.* **2010**, *150*, 296–300. [CrossRef]
125. Obraztsov, A.N. Making graphene on a large scale. *Nat. Nanotechnol.* **2009**, *4*, 212–213. [CrossRef] [PubMed]
126. Dong, X.-C.; Xu, H.; Wang, X.-W.; Huang, Y.-X.; Chan-Park, M.B.; Zhang, H.; Wang, L.-H.; Huang, W.; Chen, P. 3D Graphene–Cobalt Oxide Electrode for High-Performance Supercapacitor and Enzymeless Glucose Detection. *ACS Nano* **2012**, *6*, 3206–3213. [CrossRef] [PubMed]
127. Wang, L.; Xiong, Q.; Xiao, F.; Duan, H. 2D nanomaterials based electrochemical biosensors for cancer diagnosis. *Biosens. Bioelectron.* **2017**, *89*, 136–151. [CrossRef] [PubMed]
128. Saini, D. Synthesis and functionalization of graphene and application in electrochemical biosensing. *Nanotechnol. Rev.* **2016**, *5*, 393–416. [CrossRef]
129. Singh, R.K.; Nalajala, N.; Kar, T.; Schechter, A. *Functionalization of Graphene—A Critical Overview of its Improved Physical, Chemical and Electrochemical Properties*; Carbon Nanostructures; Springer: Cham, Switzerland, 2019.
130. Mei, X.; Meng, X.; Wu, F. Hydrothermal method for the production of reduced graphene oxide. *Phys. E Low-Dimens. Syst. Nanostruct.* **2015**, *68*, 81–86. [CrossRef]
131. Zhao, C.; Wu, X.; Zhang, X.; Li, P.; Qian, X. Facile synthesis of layered CuS/RGO/CuS nanocomposite on Cu foam for ultrasensitive nonenzymatic detection of glucose. *J. Electroanal. Chem.* **2017**, *785*, 172–179. [CrossRef]
132. Seekaew, Y.; Arayawut, O.; Timsorn, K.; Wongchoosuk, C. *Synthesis, Characterization, and Applications of Graphene and Derivatives. Carbon-Based Nanofillers and Their Rubber Nanocomposites*; Elsevier: Amsterdam, The Netherlands, 2019; pp. 259–283. [CrossRef]
133. Urhan, B.K.; Demir, Ü.; Özer, T.Ö.; Doğan, H.Ö. Electrochemical fabrication of Ni nanoparticles-decorated electrochemically reduced graphene oxide composite electrode for non-enzymatic glucose detection. *Thin Solid Films* **2020**, *693*, 137695. [CrossRef]
134. Alexander, S.; Baraneedharan, P.; Balasubrahmanyan, S.; Ramaprabhu, S. Modified graphene based molecular imprinted polymer for electrochemical non-enzymatic cholesterol biosensor. *Eur. Polym. J.* **2017**, *86*, 106–116. [CrossRef]
135. Mazaheri, M.; Aashuri, H.; Simchi, A. Three-dimensional hybrid graphene/nickel electrodes on zinc oxide nanorod arrays as non-enzymatic glucose biosensors. *Sens. Actuators B Chem.* **2017**, *251*, 462–471. [CrossRef]
136. Guan, P.; Li, Y.; Zhang, J.; Li, W. Non-enzymatic glucose biosensor based on CuO-decorated CeO2 nanoparticles. *Nanomaterials* **2016**, *6*, 159. [CrossRef]
137. Si, P.; Huang, Y.; Wang, T.; Ma, J. Nanomaterials for electrochemical non-enzymatic glucose biosensors. *RSC Adv.* **2013**, *3*, 3487. [CrossRef]
138. Sakr, M.A.; Elgammal, K.; Delin, A.; Serry, M. Performance-Enhanced Non-Enzymatic Glucose Sensor Based on Graphene-Heterostructure. *Sensors* **2019**, *20*, 145. [CrossRef] [PubMed]
139. Shen, Z.; Gao, W.; Li, P.; Wang, X.; Zheng, Q.; Wu, H.; Ma, Y.; Guan, W.; Wu, S.; Yu, Y.; et al. Highly sensitive nonenzymatic glucose sensor based on nickel nanoparticle–attapulgite-reduced graphene oxide-modified glassy carbon electrode. *Talanta* **2016**, *159*, 194–199. [CrossRef] [PubMed]

140. Darvishi, S.; Souissi, M.; Karimzadeh, F.; Kharaziha, M.; Sahara, R.; Ahadian, S. Ni nanoparticle-decorated reduced graphene oxide fornon-enzymatic glucose sensing: An experimental and modeling study. *Electrochim. Acta* **2017**, *240*, 388–398. [CrossRef]
141. Wang, L.; Zhang, Y.; Yu, J.; He, J.; Yang, H.; Ye, Y.; Song, Y. A green and simple strategy to prepare graphene foam-like three-dimensional porous carbon/Ni nanoparticles for glucose sensing. *Sens. Actuators B Chem.* **2017**, *239*, 172–179. [CrossRef]
142. Lv, W.; Jin, F.-M.; Guo, Q.; Yang, Q.-H.; Kang, F. DNA-dispersed graphene/NiO hybrid materials for highly sensitive non-enzymatic glucose sensor. *Electrochim. Acta* **2012**, *73*, 129–135. [CrossRef]
143. Yuan, B.; Xu, C.; Deng, D.; Xing, Y.; Liu, L.; Pang, H.; Zhang, D.-J. Graphene oxide/nickel oxide modified glassy carbon electrode for supercapacitor and nonenzymatic glucose sensor. *Electrochim. Acta* **2013**, *88*, 708–712. [CrossRef]
144. Subramanian, P.; Niedziolka-Jonsson, J.; Leśniewski, A.; Wang, Q.; Li, M.; Boukherroub, R.; Szunerits, S. Preparation of reduced graphene oxide–Ni(OH)2 composites by electrophoretic deposition: Application for non-enzymatic glucose sensing. *J. Mater. Chem. A* **2014**, *2*, 5525–5533. [CrossRef]
145. Zhan, B.B.; Liu, C.B.; Chen, H.P.; Shi, H.X.; Wang, L.H.; Chen, P.; Huang, W.; Dong, X.C. Free-standing electrochemical electrode-based on Ni(OH)2/3D graphene foam for nonenzymatic glucose detection. *Nanoscale* **2014**, *6*, 7424–7429. [CrossRef]
146. Amin, B.G.; Masud, J.; Nath, M. A non-enzymatic glucose sensor based on a CoNi2Se4/rGO nanocomposite with ultrahigh sensitivity at low working potential. *J. Mater. Chem. B* **2019**, *7*, 2338–2348. [CrossRef]
147. Batool, R.; Akhtar, M.A.; Hayat, A.; Han, D.; Niu, L.; Ahmad, M.A.; Nawaz, M.H. A nanocomposite prepared from magnetite nanoparticles, polyaniline and carboxy-modified graphene oxide for non-enzymatic sensing of glucose. *Microchim. Acta* **2019**, *186*, 267. [CrossRef] [PubMed]
148. Lee, J.; Adegoke, O.; Park, E.Y. High-performance biosensing systems based on various nanomaterials as signal transducers. *Biotechnol. J.* **2019**, *14*, 1800249. [CrossRef] [PubMed]
149. Rahsepar, M.; Foroughi, F.; Kim, H. A new enzyme-free biosensor based on nitrogen-doped graphene with high sensing performance for electrochemical detection of glucose at biological pH value. *Sens. Actuators B Chem.* **2019**, *282*, 322–330. [CrossRef]
150. Yang, S.; Li, G.; Wang, D.; Qiao, Z.; Qu, L. Synthesis of nanoneedle-like copper oxide on N-doped reduced graphene oxide: A three-dimensional hybrid for nonenzymatic glucose sensor. *Sens. Actuators B Chem.* **2017**, *238*, 588–595. [CrossRef]
151. Zhang, Y.; Xu, J.; Xia, J.; Zhang, F.; Wang, Z. MOF-Derived Porous Ni2P/Graphene Composites with Enhanced Electrochemical Properties for Sensitive Nonenzymatic Glucose Sensing. *ACS Appl. Mater. Interfaces* **2018**, *10*, 39151–39160. [CrossRef]
152. Khosroshahia, Z.; Karimzadeh, F.; Kharazihaa, M.; Allafchianb, A. A non-enzymatic sensor based on three-dimensional graphene foam decorated with Cu-xCu2O nanoparticles for electrochemical detection of glucose and its application in human serum. *Mater. Sci. Eng. C* **2020**, *108*, 110216. [CrossRef]
153. Zhang, Y.; Lei, W.; Wu, Q.; Xia, X.; Hao, Q. Amperometric nonenzymatic determination of glucose via a glassy carbon electrode modified with nickel hydroxide and N-doped reduced graphene oxide. *Microchim. Acta* **2017**, *184*, 3103–3111. [CrossRef]
154. Geng, D.; Bo, X.; Guo, L. Ni-doped molybdenum disulfide nanoparticles anchored on reduced graphene oxide as novel electroactive material for a non-enzymatic glucose sensor. *Sens. Actuators B Chem.* **2017**, *244*, 131–141. [CrossRef]
155. Yang, J.; Ye, H.; Zhang, Z.; Zhao, F.; Zeng, B. Metal–organic framework derived hollow polyhedron CuCo2O4 functionalized porous graphene for sensitive glucose sensing. *Sens. Actuators B Chem.* **2017**, *242*, 728–735. [CrossRef]
156. Tehrani, F.; Bavarian, B. Facile and scalable disposable sensor based on laser engraved graphene for electrochemical detection of glucose. *Sci. Rep.* **2016**, *6*, 27975. [CrossRef]
157. He, J.; Sunarso, J.; Zhu, Y.; Zhong, Y.; Miao, J.; Zhou, W.; Shao, Z. High-performance non-enzymatic perovskite sensor for hydrogen peroxide and glucose electrochemical detection. *Sens. Actuators B Chem.* **2017**, *244*, 482–491. [CrossRef]
158. Yang, J.; Lin, Q.; Yin, W.; Jiang, T.; Zhao, D.; Jiang, L. A novel nonenzymatic glucose sensor based on functionalized PDDA-graphene/CuO nanocomposites. *Sens. Actuators B Chem.* **2017**, *253*, 1087–1095. [CrossRef]

159. Zang, G.; Hao, W.; Li, X.; Huang, S.; Gan, J.; Luo, Z.; Zhang, Y. Copper nanowires-MOFs-graphene oxide hybrid nanocomposite targeting glucose electro-oxidation in neutral medium. *Electrochim. Acta* **2018**, *277*, 176–184. [CrossRef]
160. Zhang, Q.; Luo, Q.; Qin, Z.; Liu, L.; Wu, Z.; Shen, B.; Hu, W. Self-Assembly of Graphene-Encapsulated Cu Composites for Nonenzymatic Glucose Sensing. *ACS Omega* **2018**, *3*, 3420–3428. [CrossRef] [PubMed]
161. Ayranci, R.; Demirkan, B.; Sen, B.; Şavk, A.; Ak, M.; Şen, F. Use of the monodisperse Pt/Ni@rGO nanocomposite synthesized by ultrasonic hydroxide assisted reduction method in electrochemical nonenzymatic glucose detection. *Mater. Sci. Eng. C* **2019**, *99*, 951–956. [CrossRef] [PubMed]
162. Du, Y.; He, Y.; Zheng, Z.; Shen, X.; Zhou, Y.; Wang, T.; Zhu, Z.; Wang, C. A Renewable Platform for High-Performance Glucose Sensor Based on Co(OH)2 Nanoparticles/Three-Dimensional Graphene Frameworks. *J. Electrochem. Soc.* **2019**, *166*, B42–B48. [CrossRef]
163. Toi, P.T.; Trung, T.Q.; Dang, T.M.L.; Bae, C.W.; Lee, N.-E. Highly Electrocatalytic, Durable, and Stretchable Nanohybrid Fiber for On-Body Sweat Glucose Detection. *ACS Appl. Mater. Interfaces* **2019**, *11*, 10707–10717. [CrossRef]
164. Kong, F.-Y.; Li, X.-R.; Zhao, W.-W.; Xu, J.-J.; Chen, H.-Y. Graphene oxide–thionine–Au nanostructure composites: Preparation and applications in non-enzymatic glucose sensing. *Electrochem. Commun.* **2012**, *14*, 59–62. [CrossRef]
165. Liu, Y.; Dong, Y.; Guo, C.X.; Cui, Z.; Zheng, L.; Li, C.M. Protein-Directed In Situ Synthesis of Gold Nanoparticles on Reduced Graphene Oxide Modified Electrode for Nonenzymatic Glucose Sensing. *Electroanalysis* **2012**, *24*, 2348–2353. [CrossRef]
166. Wang, Q.; Cui, X.; Chen, J.; Zheng, X.; Liu, C.; Xue, T.; Wang, H.; Jin, Z.; Qiao, L.; Zheng, W. Well-dispersed palladium nanoparticles on graphene oxide as a non-enzymatic glucose sensor. *RSC Adv.* **2012**, *2*, 6245–6249. [CrossRef]
167. Wu, J.-W.; Wang, C.-H.; Wang, Y.-C.; Changb, J.-K. Ionic-liquid-enhanced glucose sensing ability of non-enzymatic Au/graphene electrodes fabricated using supercritical CO2 fluid. *Biosens. Bioelectron.* **2013**, *46*, 30–36. [CrossRef] [PubMed]
168. Wu, G.-H.; Song, X.-H.; Wu, Y.; Chen, X.; Luo, F.; Chen, X. Non-enzymatic electrochemical glucose sensor based on platinum nanoflowers supported on graphene oxide. *Talanta* **2013**, *105*, 379–385. [CrossRef] [PubMed]
169. Ismail, N.S.; Le, Q.H.; Yoshikawa, H.; Saito, M.; Tamiya, E. Development of Non-enzymatic Electrochemical Glucose Sensor Based on Graphene Oxide Nanoribbon—Gold Nanoparticle Hybrid. *Electrochim. Acta* **2014**, *146*, 98–105. [CrossRef]
170. Ruiyi, L.; Juanjuan, Z.; Zhouping, W.; Zaijun, L.; Junkang, L.; Zhiguo, G.; Wang, G.-L. Novel graphene-gold nanohybrid with excellent electrocatalytic performance for the electrochemical detection of glucose. *Sens. Actuators B Chem.* **2015**, *208*, 421–428. [CrossRef]
171. Joshi, A.C.; Markad, G.B.; Haram, S.K. Rudimentary simple method for the decoration of graphene oxide with silver nanoparticles: Their application for the amperometric detection of glucose in the human blood samples. *Electrochim. Acta* **2015**, *161*, 108–114. [CrossRef]
172. Hoa, L.T.; Sun, K.G.; Hur, S.H. Highly sensitive non-enzymatic glucose sensor based on Pt nanoparticle decorated graphene oxide hydrogel. *Sens. Actuators B Chem.* **2015**, *210*, 618–623. [CrossRef]
173. Shu, H.; Chang, G.; Su, J.; Cao, L.; Huang, Q.; Zhang, Y.; Xia, T.; He, Y. Single-step electrochemical deposition of high performance Au-graphene nanocomposites for nonenzymatic glucose sensing. *Sens. Actuators B Chem.* **2015**, *220*, 331–339. [CrossRef]
174. Luo, Y.; Kong, F.-Y.; Li, C.; Shi, J.; Lv, W.; Wang, W. One-pot preparation of reduced graphene oxide-carbon nanotube decorated with Au nanoparticles based on protein for non-enzymatic electrochemical sensing of glucose. *Sens. Actuators B Chem.* **2016**, *234*, 625–632. [CrossRef]
175. Thanh, T.D.; Balamurugan, J.; Hwang, J.Y.; Kim, N.H.; Lee, J.H. In situ synthesis of graphene-encapsulated gold nanoparticle hybrid electrodes for non-enzymatic glucose sensing. *Carbon* **2016**, *98*, 90–98. [CrossRef]
176. Fan, Z.; Liu, B.; Liu, X.; Li, Z.; Wang, H.; Yang, S.; Wang, J. A flexible and disposable hybrid electrode based on Cu nanowires modified graphene transparent electrode for non-enzymatic glucose sensor. *Electrochim. Acta* **2013**, *109*, 602–608. [CrossRef]
177. Wang, B.; Li, S.; Liu, J.; Yu, M. Preparation of nickel nanoparticle/graphene composites for non-enzymatic electrochemical glucose biosensor applications. *Mater. Res. Bull.* **2014**, *49*, 521–524. [CrossRef]

178. Wang, B.; Wu, Y.; Chen, Y.; Weng, B.; Li, C.M. Flexible paper sensor fabricated via in situ growth of Cu nanoflower on RGO sheets towards amperometrically non-enzymatic detection of glucose. *Sens. Actuators B Chem.* **2017**, *238*, 802–808. [CrossRef]
179. Wang, Z.; Hu, Y.; Yang, W.; Zhou, M.; Hu, X. Facile One-Step Microwave-Assisted Route towards Ni Nanospheres/Reduced Graphene Oxide Hybrids for Non-Enzymatic Glucose Sensing. *Sensors* **2012**, *12*, 4860–4869. [CrossRef]
180. Shackery, I.; Patil, U.; Pezeshki, A.; Shinde, N.M.; Kang, S.; Im, S.; Jun, S.C. Copper Hydroxide Nanorods Decorated Porous Graphene Foam Electrodes for Non-enzymatic Glucose Sensing. *Electrochim. Acta* **2016**, *191*, 954–961. [CrossRef]
181. Liu, M.; Liu, R.; Chen, W. Graphene wrapped Cu2O nanocubes: Non-enzymatic electrochemical sensors for the detection of glucose and hydrogen peroxide with enhanced stability. *Biosens. Bioelectron.* **2013**, *45*, 206–212. [CrossRef]
182. Wang, X.; Liu, E.; Zhang, X. Non-enzymatic glucose biosensor based on copper oxide-reduced graphene oxide nanocomposites synthesized from water-isopropanol solution. *Electrochim. Acta* **2014**, *130*, 253–260. [CrossRef]
183. Zhao, Y.; Bo, X.; Guo, L. Highly exposed copper oxide supported on three-dimensional porous reduced graphene oxide for non-enzymatic detection of glucose. *Electrochim. Acta* **2015**, *176*, 1272–1279. [CrossRef]
184. Ye, D.; Liang, G.; Li, H.; Luo, J.; Zhang, S.; Chen, H.; Kong, J. A novel nonenzymatic sensor based on CuO nanoneedle/graphene/carbon nanofiber modified electrode for probing glucose in saliva. *Talanta* **2013**, *116*, 223–230. [CrossRef] [PubMed]
185. Mei, L.-P.; Song, P.; Feng, J.-J.; Shen, J.-H.; Wang, W.; Wang, A.-J.; Weng, X. Nonenzymatic amperometric sensing of glucose using a glassy carbon electrode modified with a nanocomposite consisting of reduced graphene oxide decorated with Cu2O nanoclusters. *Microchim. Acta* **2015**, *182*, 1701–1708. [CrossRef]
186. Feng, X.; Guo, C.; Mao, L.; Ning, J.; Hu, Y. Facile Growth of Cu 2 O Nanowires on Reduced Graphene Sheets with High Nonenzymatic Electrocatalytic Activity Toward Glucose. *J. Am. Ceram. Soc.* **2013**, *97*, 811–815. [CrossRef]
187. Alizadeh, T.; Mirzagholipur, S. A Nafion-free non-enzymatic amperometric glucose sensor based on copper oxide nanoparticles–graphene nanocomposite. *Sens. Actuators B Chem.* **2014**, *198*, 438–447. [CrossRef]
188. Yazid, S.N.A.M.; Isa, I.M.; Hashim, N. Novel alkaline-reduced cuprous oxide/graphene nanocomposites for non-enzymatic amperometric glucose sensor application. *Mater. Sci. Eng. C* **2016**, *68*, 465–473. [CrossRef] [PubMed]
189. Luo, J.; Zhang, H.; Jiang, S.; Jiang, J.; Liu, X. Facile one-step electrochemical fabrication of a non-enzymatic glucose-selective glassy carbon electrode modified with copper nanoparticles and graphene. *Microchim. Acta* **2012**, *177*, 485–490. [CrossRef]
190. Luo, L.; Zhu, L.; Wang, Z. Nonenzymatic amperometric determination of glucose by CuO nanocubes–graphene nanocomposite modified electrode. *Bioelectrochemistry* **2012**, *88*, 156–163. [CrossRef]
191. Sun, C.-L.; Cheng, W.-L.; Hsu, T.-K.; Chang, C.-W.; Chang, J.-L.; Zen, J.-M. Ultrasensitive and highly stable nonenzymatic glucose sensor by a CuO/graphene-modified screen-printed carbon electrode integrated with flow-injection analysis. *Electrochem. Commun.* **2013**, *30*, 91–94. [CrossRef]
192. Yan, X.; Yang, J.; Ma, L.; Tong, X.; Wang, Y.-Y.; Jin, G.; Guo, X.-Y. Size-controlled synthesis of Cu2O nanoparticles on reduced graphene oxide sheets and their application as non-enzymatic glucose sensor materials. *J. Solid State Electrochem.* **2015**, *19*, 3195–3199. [CrossRef]
193. Hoa, L.T.; Chung, J.S.; Hur, S.H. A highly sensitive enzyme-free glucose sensor based on Co 3 O 4 nanoflowers and 3D graphene oxide hydrogel fabricated via hydrothermal synthesis. *Sens. Actuators B Chem.* **2016**, *223*, 76–82. [CrossRef]
194. Heidari, H.; Habibi, E. Amperometric enzyme-free glucose sensor based on the use of a reduced graphene oxide paste electrode modified with electrodeposited cobalt oxide nanoparticles. *Microchim. Acta* **2016**, *183*, 2259–2266. [CrossRef]
195. Li, S.-J.; Du, J.-M.; Chen, J.; Mao, N.-N.; Zhang, M.-J.; Pang, H. Electrodeposition of cobalt oxide nanoparticles on reduced graphene oxide: A two-dimensional hybrid for enzyme-free glucose sensing. *J. Solid State Electrochem.* **2013**, *18*, 1049–1056. [CrossRef]

196. Sun, J.-Y.; Huang, K.; Fan, Y.; Wu, Z.-W.; Li, D.-D. Glassy carbon electrode modified with a film composed of Ni(II), quercetin and graphene for enzyme-less sensing of glucose. *Microchim. Acta* **2011**, *174*, 289–294. [CrossRef]
197. Belkhalfa, H.; Teodorescu, F.; Quéniat, G.; Coffinier, Y.; Dokhan, N.; Sam, S.; Abderrahmani, A.; Boukherroub, R.; Szunerits, S. Insulin impregnated reduced graphene oxide/Ni(OH)2 thin films for electrochemical insulin release and glucose sensing. *Sens. Actuators B Chem.* **2016**, *237*, 693–701. [CrossRef]
198. Zhang, H.; Liu, S. Nanoparticles-assembled NiO nanosheets templated by graphene oxide film for highly sensitive non-enzymatic glucose sensing. *Sens. Actuators B Chem.* **2017**, *238*, 788–794. [CrossRef]
199. Zhang, Y.; Xu, F.; Sun, Y.; Shi, Y.; Wen, Z.; Li, Z. Assembly of Ni(OH)2 nanoplates on reduced graphene oxide: A two dimensional nanocomposite for enzyme-free glucose sensing. *J. Mater. Chem.* **2011**, *21*, 16949–16954. [CrossRef]
200. Qiao, N.; Zheng, J. Nonenzymatic glucose sensor based on glassy carbon electrode modified with a nanocomposite composed of nickel hydroxide and graphene. *Microchim. Acta* **2012**, *177*, 103–109. [CrossRef]
201. Zhu, X.; Jiao, Q.; Zhang, C.; Zuo, X.; Xiao, X.; Liang, Y.; Nan, J. Amperometric nonenzymatic determination of glucose based on a glassy carbon electrode modified with nickel(II) oxides and graphene. *Microchim. Acta* **2013**, *180*, 477–483. [CrossRef]
202. Ye, Y.; Wang, P.; Dai, E.; Liu, J.; Tian, Z.; Liang, C.; Shao, G. A novel reduction approach to fabricate quantum-sized SnO2-conjugated reduced graphene oxide nanocomposites as non-enzymatic glucose sensors. *Phys. Chem. Chem. Phys.* **2014**, *16*, 8801–8807. [CrossRef]
203. Xiao, F.; Li, Y.-Q.; Gao, H.; Ge, S.; Duan, H. Growth of coral-like PtAu–MnO2 binary nanocomposites on free-standing graphene paper for flexible nonenzymatic glucose sensors. *Biosens. Bioelectron.* **2013**, *41*, 417–423. [CrossRef]
204. Wang, L.; Lu, X.; Ye, Y.; Sun, L.; Song, Y. Nickel-cobalt nanostructures coated reduced graphene oxide nanocomposite electrode for nonenzymatic glucose biosensing. *Electrochim. Acta* **2013**, *114*, 484–493. [CrossRef]
205. Dhara, K.; Stanley, J.; Ramachandran, T.; Nair, B.G.; Tg, S.B. Pt-CuO nanoparticles decorated reduced graphene oxide for the fabrication of highly sensitive non-enzymatic disposable glucose sensor. *Sens. Actuators B Chem.* **2014**, *195*, 197–205. [CrossRef]
206. Li, M.; Bo, X.; Mu, Z.; Zhang, Y.; Guo, L. Electrodeposition of nickel oxide and platinum nanoparticles on electrochemically reduced graphene oxide film as a nonenzymatic glucose sensor. *Sens. Actuators B Chem.* **2014**, *192*, 261–268. [CrossRef]
207. Yuan, M.; Liu, A.; Zhao, M.; Dong, W.; Zhao, T.; Wang, J.; Tang, W. Bimetallic PdCu nanoparticle decorated three-dimensional graphene hydrogel for non-enzymatic amperometric glucose sensor. *Sens. Actuators B Chem.* **2014**, *190*, 707–714. [CrossRef]
208. Hu, Y.; He, F.; Ben, A.; Chen, C. Synthesis of hollow Pt–Ni–graphene nanostructures for nonenzymatic glucose detection. *J. Electroanal. Chem.* **2014**, *726*, 55–61. [CrossRef]
209. Li, M.; Bo, X.; Zhang, Y.; Han, C.; Guo, L. One-pot ionic liquid-assisted synthesis of highly dispersed PtPd nanoparticles/reduced graphene oxide composites for nonenzymatic glucose detection. *Biosens. Bioelectron.* **2014**, *56*, 223–230. [CrossRef] [PubMed]
210. Chen, X.; Tian, X.; Zhao, L.; Huang, Z.-Y.; Oyama, M. Nonenzymatic sensing of glucose at neutral pH values using a glassy carbon electrode modified with graphene nanosheets and Pt-Pd bimetallic nanocubes. *Microchim. Acta* **2013**, *181*, 783–789. [CrossRef]
211. Ensafi, A.A.; Ahmadi, Z.; Jafari-Asl, M.; Rezaei, B. Graphene nanosheets functionalized with Nile blue as a stable support for the oxidation of glucose and reduction of oxygen based on redox replacement of Pd-nanoparticles via nickel oxide. *Electrochim. Acta* **2015**, *173*, 619–629. [CrossRef]
212. Dhara, K.; Ramachandran, T.; Nair, B.G.; Babu, T.S. Single step synthesis of Au–CuO nanoparticles decorated reduced graphene oxide for high performance disposable nonenzymatic glucose sensor. *J. Electroanal. Chem.* **2015**, *743*, 1–9. [CrossRef]
213. Dhara, K.; Thiagarajan, R.; Nair, B.G.; Babu, T.S. Highly sensitive and wide-range nonenzymatic disposable glucose sensor based on a screen printed carbon electrode modified with reduced graphene oxide and Pd-CuO nanoparticles. *Microchim. Acta* **2015**, *182*, 2183–2192. [CrossRef]

214. Lu, L.; Li, H.; Qu, F.; Zhang, X.; Shen, G.-L.; Yu, R.-Q. In situ synthesis of palladium nanoparticle–graphene nanohybrids and their application in nonenzymatic glucose biosensors. *Biosens. Bioelectron.* **2011**, *26*, 3500–3504. [CrossRef]
215. Yang, J.; Yu, J.-H.; Strickler, J.R.; Chang, W.-J.; Gunasekaran, S. Nickel nanoparticle–chitosan-reduced graphene oxide-modified screen-printed electrodes for enzyme-free glucose sensing in portable microfluidic devices. *Biosens. Bioelectron.* **2013**, *47*, 530–538. [CrossRef]
216. Wang, L.; Zheng, Y.; Lu, X.; Li, Z.; Sun, L.; Song, Y. Dendritic copper-cobalt nanostructures/reduced graphene oxide-chitosan modified glassy carbon electrode for glucose sensing. *Sens. Actuators B Chem.* **2014**, *195*, 1–7. [CrossRef]
217. Hui, N.; Wang, S.; Xie, H.; Xu, S.; Niu, S.; Luo, X. Nickel nanoparticles modified conducting polymer composite of reduced graphene oxide doped poly(3,4-ethylenedioxythiophene) for enhanced nonenzymatic glucose sensing. *Sens. Actuators B Chem.* **2015**, *221*, 606–613. [CrossRef]
218. Farid, M.M.; Goudini, L.; Piri, F.; Zamani, A.; Saadati, F. Molecular imprinting method for fabricating novel glucose sensor: Polyvinyl acetate electrode reinforced by MnO2/CuO loaded on graphene oxide nanoparticles. *Food Chem.* **2016**, *194*, 61–67. [CrossRef]
219. Jiang, D.; Liu, Q.; Wang, K.; Qian, J.; Dong, X.; Yang, Z.; Du, X.; Qiu, B. Enhanced non-enzymatic glucose sensing based on copper nanoparticles decorated nitrogen-doped graphene. *Biosens. Bioelectron.* **2014**, *54*, 273–278. [CrossRef]
220. Balamurugan, J.; Thanh, T.D.; Heo, S.-B.; Kim, N.H.; Lee, J.H. Novel route to synthesis of N-doped graphene/Cu–Ni oxide composite for high electrochemical performance. *Carbon* **2015**, *94*, 962–970. [CrossRef]
221. Yang, S.; Li, G.; Wang, G.; Zhao, J.; Gao, X.; Qu, L. Synthesis of Mn3O4 nanoparticles/nitrogen-doped graphene hybrid composite for nonenzymatic glucose sensor. *Sens. Actuators B Chem.* **2015**, *221*, 172–178. [CrossRef]
222. Yang, S.; Liu, L.; Wang, G.; Li, G.; Deng, D.; Qu, L. One-pot synthesis of Mn3O4 nanoparticles decorated with nitrogen-doped reduced graphene oxide for sensitive nonenzymatic glucose sensing. *J. Electroanal. Chem.* **2015**, *755*, 15–21. [CrossRef]